







Article

Sustainable Production of Biodiesel from Novel Non-Edible Oil Seeds (*Descurainia sophia* L.) via Green Nano CeO₂ Catalyst

Maryam Tanveer Akhtar ¹, Mushtaq Ahmad ^{2,3,*}, Mohamed Fawzy Ramadan ⁴, Trobjon Makhkamov ⁵, Akramjon Yuldashev ⁶, Oybek Mamarakhimov ⁷, Mamoona Munir ⁸, Maliha Asma ¹, Muhammad Zafar ² and Salman Majeed ^{2,9}

¹ Department of Environmental Science, International Islamic University, Islamabad 44000, Pakistan

² Department of Plant Sciences, Quaid-i-Azam University Islamabad, Islamabad 45320, Pakistan

³ Pakistan Academy of Sciences, Islamabad 46000, Pakistan

⁴ Department of Clinical Nutrition, Faculty of Applied Medical Sciences, Umm Al-Qura University, Makkah 21961, Saudi Arabia

⁵ Department of Forestry and Landscape Design, Tashkent State Agrarian University, 2 A., Universitet Str., Kibray District, Tashkent 100700, Uzbekistan

⁶ Department of Ecology and Botany, Andijan State University, 129, Universitet Str., Andijan 170100, Uzbekistan

⁷ Department of Ecology Monitoring, National University of Uzbekistan, 4 University Street, Tashkent 100174, Uzbekistan

⁸ Department of Botany, Rawalpindi Women University, Satellite Town, Rawalpindi 46300, Pakistan

⁹ Department of Botany, University of Mianwali, Mianwali 42200, Pakistan

* Correspondence: mushtaq@qau.edu.pk

Abstract: The current study focuses on the synthesis of Cerium oxide (CeO₂) nanocatalyst via Tragacanth Gum (TG) using the wet impregnation method and its application for sustainable biodiesel production from a novel, non-edible *Descurainia sophia* (L.) Webb ex Prantl seed oil. The *D. sophia* seed oil has higher oil content (36 wt%) and free fatty acid (FFA) value (0.6 mg KOH/g). Innovative analytical methods, such as X-ray diffraction (XRD), scanning electron microscopy (SEM), energy dispersive X-ray (EDX), transmission electron microscopy (TEM), thermogravimetric analysis (TGA), and Fourier transform infrared spectroscopy, were used to characterize the newly synthesized, environmentally friendly, and recyclable CeO₂-TG phytonanocatalyst (FT-IR). The results show that the CeO₂-TG phytonanocatalyst was 22 nm in diameter with a spherical shape outer morphology, while the inner structure was hexagonal. Due to low FFA content, the *D. sophia* seed oil was pretreated and transesterified via a single step. Using varying parameters, the optimized process variables were determined via Response Surface Methodology (RSM). The optimum process values were 8:1 methanol to oil molar ratio, 0.3 wt% catalyst concentration, 90 °C temperature, and reaction time of 210 min with 98% biodiesel yield. The recently created phytonanocatalyst was reliable and effective, with three times reusability in the transesterification reaction. Thin layer chromatography (TLC), FT-IR, gas chromatography–mass spectroscopy (GCMS), and Nuclear magnetic resonance (NMR) analyses were used to characterize the synthesized biodiesel. Physico-chemical properties of *D. sophia* biodiesel, i.e., Kinematic viscosity (4.23 mm²/s), density (0.800 kg/m³), pour point (−7 °C), cloud point (−12 °C), and flash point (73.5 °C) agree well with international biodiesel standards (ASTM-6751, 951), (EU-14214), and China (GB/T 20828) standards. The results show that the synthesized nanocatalyst demonstrated remarkable stability, indicating a bright future for industrial biodiesel production from low-cost feedstock.

Keywords: non-edible seed oil; phytonanocatalyst; response surface methodology; catalyst reusability; physicochemical properties

1. Introduction

The energy consumption rate is increasing throughout the world. The projected energy requirement will be higher than 50% by 2030 than today [1]. The industrial and automobile



Citation: Akhtar, M.T.; Ahmad, M.; Ramadan, M.F.; Makhkamov, T.; Yuldashev, A.; Mamarakhimov, O.; Munir, M.; Asma, M.; Zafar, M.; Majeed, S. Sustainable Production of Biodiesel from Novel Non-Edible Oil Seeds (*Descurainia sophia* L.) via Green Nano CeO₂ Catalyst. *Energies* **2023**, *16*, 1534. <https://doi.org/10.3390/en16031534>

Academic Editor: João Fernando Pereira Gomes

Received: 20 December 2022

Revised: 17 January 2023

Accepted: 24 January 2023

Published: 3 February 2023



Copyright: © 2023 by the authors. Licensee MDPI, Basel, Switzerland. This article is an open access article distributed under the terms and conditions of the Creative Commons Attribution (CC BY) license (<https://creativecommons.org/licenses/by/4.0/>).

sector highly depends on fossil fuels [2]. Fossil fuels release greenhouse gasses and CO₂ emissions into the atmosphere, causing global warming. Therefore, the rising crude oil prices, global climate change, energy security concerns, exhaustion of fossil fuel reserves, and degradation of land and water fossil fuel sources have compelled governments, policy-makers, scientists, and researchers to discover alternative energy sources [3]. Researchers have focused on biodiesel as a potential alternative fuel among the contenders.

Biodiesel is a reusable, non-poisonous, degradable, and ecologically sustainable fuel [4] consisting of a mixture of alkyl esters of long-chain fatty acids generated from free fatty acids and triglycerides through the esterification and transesterification processes [5,6]. BD has a higher oxygen concentration than petroleum diesel, which gives it a competitive advantage over the latter [4]. The 20% biodiesel blend with diesel lowers smoke, CO, and hydrocarbon emissions [7]. Potential sources for biodiesel feedstock include edible oils, such as soybean, coconut, rapeseed, and sunflower, as first-generation feedstock and second-generation feedstock, i.e., non-edible vegetable oils, e.g., jatropha, palm, castor bean, waste oil, as well as animal fats [8]. Third-generation feedstock includes algae, fungi, microalgae, bacteria, and terpenes [5]. Several concerns associated with using first-generation feedstock, such as high production cost, deforestation, and food versus fuel debate, are the leading causes of its commercialization. Finding non-edible oil resources (second-generation feedstock) is essential to controlling this problem because they can be cost-effective and help with food shortages. Therefore, it makes sense to develop alternative renewable oils that not only enhance the economic feasibility of biofuel but also increase the probability of such fuels being produced [9].

D. sophia is an annual herbaceous oil-yielding plant of the Brassicaceae family and is commonly named flixweed. *D. sophia* is widely distributed globally and is mainly found in Asia, South Africa, North America, New Zealand, and Southern Europe. In Pakistan, it is mainly distributed in South Waziristan and Baluchistan and grows in terrains, fodder plains, pasturelands, and farms. The plant grows up to 80 cm with hairy outgrowth from the epidermis and unbranched or distally branched stems; its leaves are ovate, oblong to ovate in outline; entire margins and pale yellow flowers are arranged in terminal clusters. The flowering period starts from April till June. A batch of 20–40 seeds is arranged in the chamber in the form of a row, oblong and reddish brown. In Persian documents, it is cited as Khaksheer, Todri, Khobbah, and Bazr-al-khomkhom. It is extensively used in folk medicines in different countries, including India, China, and Iran. However, the high amount of Erucic acid and FFA in seed oil makes it unsafe for human consumption [10].

The main techniques for producing biodiesel from physicochemical processes include pyrolysis, blending, microemulsions, and transesterification. Transesterification is the most commonly used method for producing biodiesel, in which triglycerides react with an alcoholic substance in the presence of a suitable catalyst. The most often utilized alcohol is methanol due to its low boiling point, cost economics, and no azeotrope formation [11]. The catalytic transesterification reaction is carried out by adding a suitable catalyst (homogeneous, heterogeneous, or enzyme catalyst) to the reaction mixture [12]. According to the literature, homogeneous catalysts have high catalytic efficiency, but their use in large-scale biodiesel synthesis is hampered by equipment corrosion, the difficulty of recovering the catalyst, and the wastewater production [4]. However, the problems with using heterogeneous catalysts include prolonged reactions, high reaction temperatures, and leaching of catalytic active sites [13]. Enzyme catalysts are employed to synthesize biodiesel, but this process is expensive, labor-intensive, and has a limited number of catalyst reuses. In addition, the enzymatic reaction produces a relatively low biodiesel yield, making it less economical [14].

With the advent of nanotechnology, biodiesel yield and quality are improving using nanocatalysts. Nanoparticles with various morphologies and cross-sections of fewer than 100 nm are used to create nanocatalysts. It reduced the reaction time and temperature and improved the porosity and catalytic active sites [15]. Some methods used for nanocatalyst synthesis include hydrothermal, solvothermal, sol-gel technology, microwave combus-

tion, impregnation, chemical vaporization, etc. Many different nanocatalysts have been extensively used to manufacture biodiesel from non-edible feedstock [16] of synthesized KF/CaO-Fe₃O₄ nanocatalysts for biofuel generation from the seeds of *Sitillingia*. Baskar et al. [17] made biodiesel from *Ricinus communis* oil with a high FFA level using a Ni-doped ZnO nanocatalyst. The catalyst could be reused three times. The support plays a vital role in influencing the catalytic activity of a catalyst. It is worth noting here that the composition of the support has a significant impact on the interface and electron transfer capabilities of the catalyst. These substances are required for stability, and catalytic activity is required to prevent leaching. Several works on using CeO₂ metal oxide on support have been described in the literature [18] using the soft template method for CuO-CeO₂ synthesis for biodiesel production. The catalyst reusability shows maximum biodiesel yield attained till two reaction cycles. Ebadinezhad et al. [19] created a carbon-templated meso-design of nanostructured CeAPSO-34 for biodiesel generation from FFA and waste oil. The catalyst was useable for five successive cycles.

The capacity of CeO₂ to quickly switch between the Ce⁺³ and Ce⁺⁴ states is credited with the substance's performance in various scientific fields. Cerium oxide (CeO₂) is poorly thermostable on its own, and at high temperatures, its catalytic activity decreases due to sintering, drastically altering the pore surface volume [20]. However, the enhanced texture stability of plant exudates is used as a support. It is a green synthesis method that eliminates hazardous substances in synthesizing chemical products. This study focused on the biosynthesis of CeO₂ nanoparticles via *Tragacanth Gum* (TG) as a suitable substance due to its reductive nature in nanocatalyst synthesis, followed by a simple wet impregnation route. TG is a naturally occurring acidic polysaccharide from *Astragalus gummifer* (Fabaceae) manufactured in Iran and Turkey. It is renewable, available, and safe [21]. Compositional analysis shows that TG consists of minerals (1.8–3.2% *w/w*), moisture (8.79–12.94% *w/w*), carbohydrate (83.81–86.52% *w/w*), and protein (0.31–3.82% *w/w*). A highly viscous gel-like structure is formed following swelling by the primary TG fractions, tragacanthin (water-soluble) and bassorin (water-insoluble), which differ from this composition [22].

The comprehensive literature study reported no previous work on biodiesel synthesis from *Descurainia sophia* L. Webb ex Prantl seed oil using TG modified CeO₂ nanocatalyst. However, the current study attempted to explore the potential of *Descurainia sophia* (L.) seed oil for efficient and high-quality biodiesel synthesis from powerful oxidizing and recyclable TG-modified CeO₂ nanocatalyst. As the novelty of the work, the selected feedstock and green nanocatalyst is the first time attempt to evaluate its potential for the biodiesel industry. The catalyst synthesis was examined using XRD, SEM, EDX, TEM, TGA, and FT-IR. Furthermore, the effects of functionalized parameters on biofuel yield, i.e., catalyst weight %, process time, temperature, and molar ratio, were evaluated via RSM-CCD. The biodiesel synthesis was checked through TLC, FTIR, GCMS, and NMR techniques. The TG-modified CeO₂ nanocatalyst reusability and stability were also evaluated. Finally, the optimized biodiesel sample was further analyzed to determine its fuel properties compared with international standards of biofuel, American (ASTM 6751, 951), European Union (EN 14214), and China GB/T 20, 828 (2007).

2. Materials and Methods

Descurainia sophia L. Webb ex Prantl seeds were collected during multiple trips across Pakistan. The seeds were dried in sunlight, then in the oven at 60 °C for 24 h to remove moisture and crushed into fine powder to determine the seed oil content. TG was acquired from a local market in Rawalpindi, Pakistan. All the chemicals, including n-hexane, isopropanol, phenolphthalein, Cerium Oxide (CeO₂), Sodium Hydroxide (NaOH), methanol (CH₃OH), and Sodium dodecyl sulfate, were purchased from Sigma-Aldrich (St. Louis, MO, USA) and Merck (Darmstadt, Germany) without purification. The deionized water was used to prepare the solution.

2.1. Preliminary Study of Feedstock

D. sophia L. seed oil was extracted using chemical and mechanical oil extractors. In the chemical oil extraction process, a known amount of seed powder (10 g) was subjected in a soxhlet extractor flask (VWR VELP Scientifica, Furtwangen, Germany), placed in a thimble, and round bottom (250 mL) flask was fitted under it was filled up with *n*-hexane for 8 h at 60 °C. A rotary evaporator was used for the separation of oil from *n*-hexane. The powdered sample was kept in an oven to evaporate the remaining organic solvent. Triplicate trials were performed for extraction, and the oil content was calculated using Equation (1) [23].

$$\text{Crude oil \% (W4)} = (W3 - W1) / W2 \times 100 \quad (1)$$

where *W*1 is empty flask weight, *W*2 is powdered sample + empty flask weight, *W*3 is the weight of sample used, and *W*4 is the weight of extracted oil.

Oil was extracted from a large number of seeds of *D. sophia* using a mechanical expeller (KEK P0015, 10127 Germany) and then stored in an airtight bottle to avoid photo-oxidation of oil.

The volumetric titration method determined the FFA value of *D. sophia* oil. When the endpoint (pink color) was reached, a known volume of crude *D. sophia* oil was combined with isopropyl alcohol and titrated against a solution of 0.025 M KOH. Phenolphthalein was used as the final point indicator. Sample and blank titration were performed. The mean volume of FFA of crude oil was calculated as shown in Equation (2) [24].

$$\text{Acid Value} = \frac{\text{sample titration volume} - \text{blank titration volume}}{\text{total volume of oil used}} \times \text{catalyst mass (g/L)} \quad (2)$$

2.2. Nanocatalyst Synthesis

The green/biological wet impregnation route was followed for the green synthesis of nanocatalysts with some modifications [13]. Preparing a homogenous Tragacanth Gum stock solution involved adding a specified quantity of TG to distilled water at a temperature of 70 °C. The solution was repeatedly heated and stirred until it became transparent. This solution was centrifuged to remove impurities, and the supernatant was separated. Then, 1 mM aqueous solution of CeO₂ was prepared, then mixed with a supernatant of TG and refluxed at 600 rpm for 7 h. The obtained sample was oven-dried at 120 °C, followed by calcination for 3 h at 500 °C and ground into fine powder for characterization [25].

2.3. Characterization of Synthesized Nanocatalyst

Different tests were analyzed for various physicochemical properties of prepared TG-modified CeO₂ nanocatalysts. The surface morphology of the TG-modified CeO₂ nanocatalyst was studied using SEM, Model KYKY Em-6900. The sample was coated with Palladium and Gold with 2 kv accelerating voltage. An SEM was equipped with an Energy Dispersive X-ray (EDX) (BRUKER, Billerica, MA, USA) to examine chemical composition. The crystallinity behavior of the synthesized nanocatalyst was recorded using D8 Advanced BRUKER with Cu K α radiations (0.1541 nm) over 2 θ from 10–70° with 2°/min at 45 kV and 40 mA. The average particle size was computed using the Debye–Scherer equation. The inner surface morphology of the CeO₂-modified TG nanocatalyst was analyzed via Transmission Electron Microscopy (TEM) Model (JEM-200CX). Functional groups of nanocatalysts were analyzed through FT-IR (BRUKER) with a spectral range of 4000–500 cm⁻¹. Thermogravimetric (TGA) and differential thermal analysis (DTA) (STAR^e SW 12.10) were used to examine the nanocatalyst behavior against temperature under a flow rate of dry air with temperature ranges (0–900 °C) and heating rate of 10 °C/min.

2.4. Biodiesel Production and Analysis

In a 250 mL round bottom flask equipped with a thermostat, magnetic stirrer, and reflux condenser with an oil sample outlet, *D. sophia* oil preheated to 60 °C (50 mL) was added. A suitable amount of nanocatalyst was added and stirred consistently using 600 rpm.

The varied reaction parameters include a catalyst concentration of 0.1–0.5 wt%, oil to methanol molar ratio of 1:2–1:10, a reaction time of 30–360 min, and a reaction temperature of 30–150 °C. The reaction mixture was allowed to settle overnight in a separating funnel. The upper phase contained biodiesel glycerol, and unreacted methanol was found in the lower phase. Separated biodiesel was centrifuged at 4000 rpm for 10 min. The extra methanol was taken out of the biodiesel using a rotatory evaporator. The percentage yield of biodiesel was calculated from Equation (3) [23].

$$\text{Biodiesel yield (\%)} = \frac{\text{Mass of biodiesel (g)}}{\text{Mass of oil taken (g)}} \times 100 \quad (3)$$

The *D. sophia* biodiesel sample was analyzed using thin layer chromatography (TLC) utilizing solvents (acetic acid, *n*-hexane, and diethyl ether) with a ratio (8:1:30). Iodine vapor stain was used to identify the areas of methyl esters and triglycerides that corresponded to each other [26]. Equation (4) was used to determine the TLC results [13].

$$R_f = \frac{\text{Distance traveled by sample}}{\text{Distance traveled by solvent front}} \quad (4)$$

To ascertain and validate the process of converting triglycerides into biodiesel, *R_f* (retention factor) was used. The *R_f* value of seed oil falls within the permitted range, supporting biodiesel synthesis (0.20–0.35).

FT-IR technique using DERKIN ELMER (Waltham, MA, USA), Spectrum 65 was applied to study the functional groups (vibrational motion of atoms and molecules) present in the oil and biodiesel sample in spectrum region (4000–500 cm⁻¹) at a scanning rate of 15 with 1 cm⁻¹ resolution. The composition of the synthesized biodiesel was determined using GCMS using (GC-QP 2010) ultra by SHIMADZU (Kyoto, Japan), with a capillary column of 30–0.32 mm and a film thickness of 0.25 μm. The carrier gas (Helium) was engaged at 1.70 mL/min, with 130 °C to 300 °C programmed at 80 °C/min. Avan CE 300 MHz spectrometer with 5 mm BB probes, 30 s pulse duration, 1.89 s recycle delay, and 160 scans were used to undertake (¹H NMR) and (¹³C NMR) spectra of biodiesel. Tetramethylsilane (TMS) and deuterated chloroform (CDCl₃) were used as solvents. Standard procedures (ASTM-6751, 951, EN-14214, and China GB/T 20828-2007) were followed to evaluate the physicochemical properties.

2.5. Experimental Design for Optimization Process

Optimizing the transesterification reaction parameters, including catalyst concentration, reaction temperature, oil-to-methanol molar ratio, and reaction time, was done using an experimental design based on Response Surface Methodology (RSM) and Central Composite Design (CCD) (Design Expert 13, Stat-Ease Inc., Minneapolis, MN, USA). The goal was to achieve the highest biodiesel yield possible. Thirty experimental runs were carried out based on the system-generated matrix, and ANOVA was used to extract the coefficients of the quadratic polynomial model from the experimental data. Correlation coefficients, such as adjusted R² and anticipated R², were used to investigate model validity. At the same time, statistical significance was analyzed via *p*-test. The quadratic polynomial Equation (5) indicated the calculated response (*Y*).

$$Y = \beta_0 + \sum_{i=1}^k \beta_i X_i + \sum_{i=1}^k \beta_{ii} X_i^2 + \sum_{i=1, i < j}^k \beta_{ij} X_i X_j + e \quad (5)$$

2.6. Physicochemical Properties Evaluation of Biodiesel

The key physicochemical properties of DS FAMES were assessed using the ASTM D-6751, 951 (American Standard for Testing and Materials), EN 14214 (European Union), and China GB/T 20828 standards (2007).

2.7. Catalyst Reusability Evaluation

The optimum reaction efficiency was used to assess the reusability of the TG-CeO₂ nanocatalyst. The spent catalyst was separated via centrifugation (3000 rpm for 10 min) and followed up with an *n*-hexane solvent wash to eradicate the unreactive oil and glycerol. The washed nanocatalyst was oven-dried overnight at 60 °C, followed by calcination at 500 °C for 3 h. The activated nanocatalyst in the next reaction cycles with the same reaction conditions.

3. Results and Discussion

3.1. *D. sophia* Seed Oil and FFA Content

The literature has noted that feedstocks with oil contents greater than 20% should only be used for the industrial-scale synthesis of sustainable biodiesel. In the present study, the selected novel, non-edible *D. sophia* seeds have oil content (36 wt%) which is considerably higher and recommended for biodiesel synthesis at the commercial scale. The oil FFA level was also determined before adding *D. sophia* seed oil to biodiesel. The FFA content was 0.6 mg KOH/g, as reported. So, the lower FFA of oil favors single-step transesterification. Biodiesel yield and quality highly depend upon the FFA contents of crude oil. According to previous studies, crude oil FFA content up to 2.5–3% is suitable for methyl esters production [23]. The productivity of crude oil gradually decreases as the FFA contents limit up to 3%, causing saponification and difficulty separating biodiesel.

3.2. Characterization of TG-CeO₂ Nanocatalyst

3.2.1. XRD Analysis

XRD spectrum of TG-CeO₂ nanocatalyst (Figure 1) shows that four distinct diffraction peaks appear at $2\theta = 28.62^\circ$, 33.15° , 47.52° , and 56.36° and can be indexed to (111), (200), (220), and (311) lattice planes of cube. The attained sharp peaks at 28.62° , 47.52° , and 56.36° corresponded to *d*-values of 3.11 Å, 1.91 Å, and 1.63 Å, respectively, revealed by Joint Committee on Powder Diffraction Standards (JCPDS No. 01-078-0694). The lack of additional impurity-related peaks in the XRD spectra suggests that the wet impregnation approach is used to create a pure TG-CeO₂ nanocatalyst. The diffraction peak intensity corresponds to the (111) plane 100% and is the preferred orientation plane for the CeO₂ crystal lattice. The average crystallite diameter of a more intensified peak (111) was computed via Debye Scherrer Equation (6) [27].

$$D = k\lambda / \beta \cos\theta \quad (6)$$

In this equation, *D* stands for the crystallite size (nm), the Cu-K radiation's x-ray wavelength, *k* for the form factor, the full width at half maximum, and Bragg's angle. The average crystalline size was found to be 22 nm. Navada et al. [28] analyzed phytofunctionalized CeO₂ nanoparticles mediated from *Scoparia dulcis* plant leaves. The XRD spectra match the JCPDS card with the cubic structure. The diffraction peaks show no other additional peaks and impurity peaks. Ahmad et al. [29] synthesized CeO₂ nanocatalyst using *moringa tinctoria* plant leaves. The diffraction peaks observed at 2θ values, i.e., 28.6° , 33.15° , 47.55° , 56.4° , 59.2° , and 69.55° correspond to the (*h k l*) planes of (111), (200), (220), (311), (222), and (400), respectively. The nanoparticle's crystallite size was found to be 21 nm. This study's XRD pattern of the TG-CeO₂ nanocatalyst is fairly close to the published literature studies.

3.2.2. Morphological Evaluation and Elemental Analysis

The SEM image of pure Tragacanth Gum with a less porous and filamentary surface is presented in Figure 2a. However, the SEM micrograph of TG-modified CeO₂ nanoparticles (Figure 2b) shows a spherical shape with a more porous and large surface area, increasing its active catalytic sites. The newly synthesized TG-CeO₂ nanoparticles are uniformly distributed on the surface of Tragacanth Gum and exhibit a strong locking pattern within the gum matrix. This clearly shows that the reduced metal ions get attached to the surface of

the TG matrix [30]. Anjum et al. [31] analyzed the surface morphology of Pd nanoparticles using Guar gum as a stabilizer. The SEM study verified that the nanoparticles synthesized have a roughly porous spherical shape. Ahmad et al. [29] analyzed the surface structure of green synthesized CeO_2 nanocatalysts. The pure CeO_2 showed a spherical and conjoint spherical shape structure. The conjoint and agglomeration were observed due to the presence of plant molecules. The literature review well supports the findings of the current study. The newly synthesized TG-modified CeO_2 nanocatalyst can be used for the efficient conversion of crude oil into biodiesel.

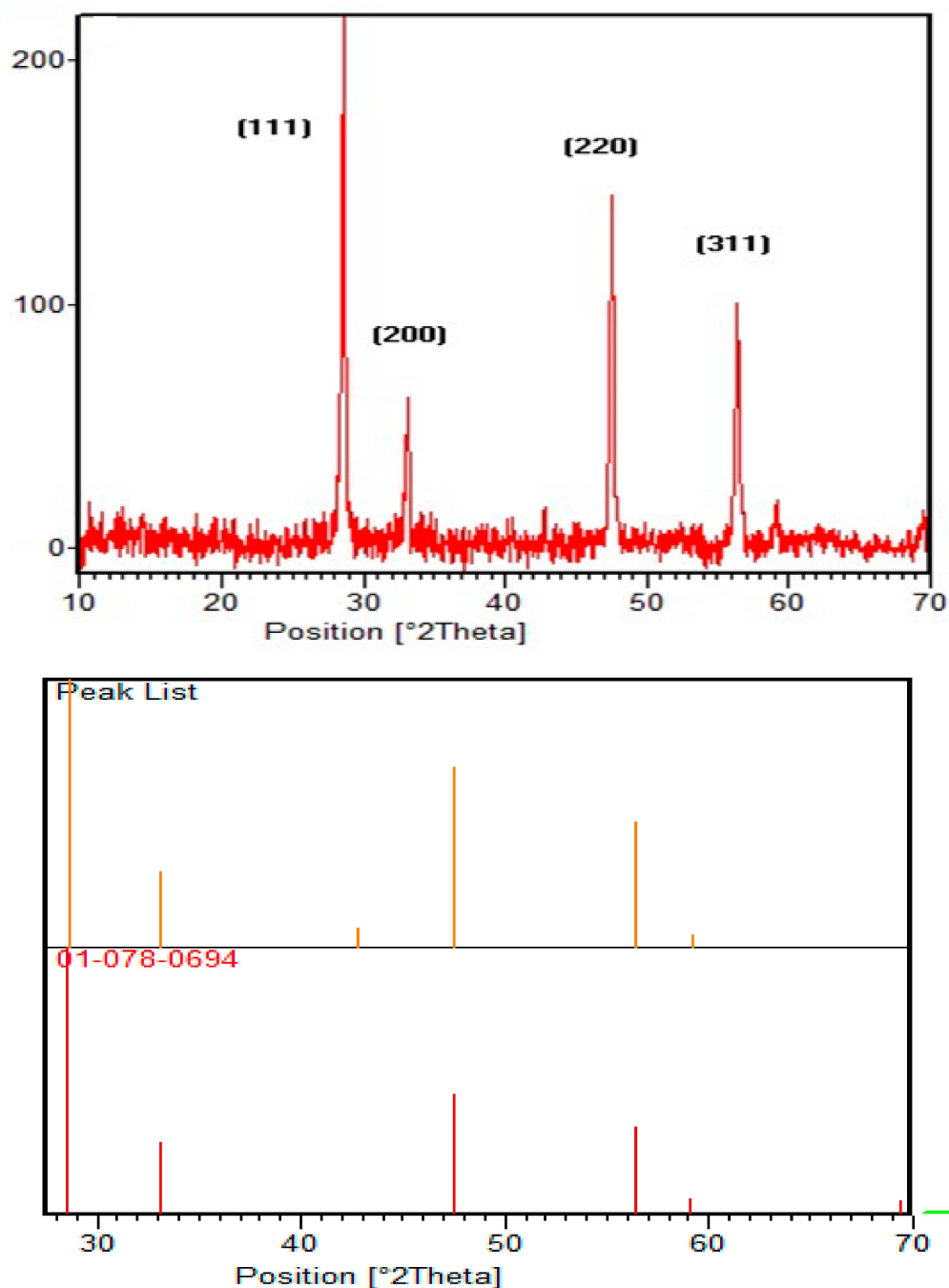


Figure 1. XRD pattern of TG-CeO₂ phytonanocatalyst with simulated reference pattern.

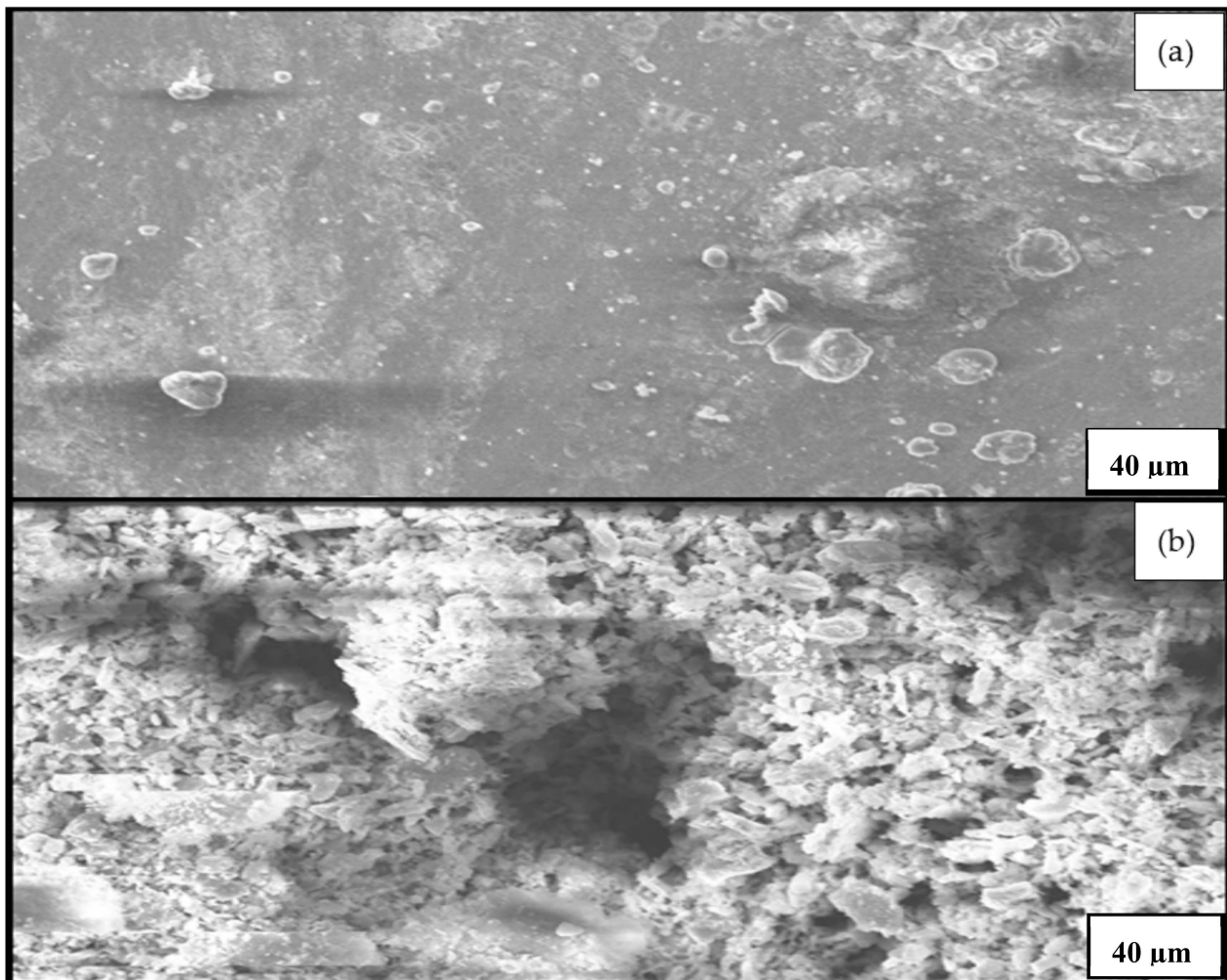


Figure 2. SEM micrographs of (a) TG (b) TG-CeO₂.

The EDX spectrum of the CeO₂ nanocatalyst is shown in Figure 3. The sharp peaks appear at 0.3 KeV, and 6.8 KeV confirms the presence of cerium (Ce); carbon (C) and Oxygen (O) elements were observed at 0.2 KeV and 0.6 KeV, respectively. Additionally, the carbon peak confirmed the presence of organic compound in TG [31]. The presence of oxygen is attributed due to CeO₂. The elemental composition of synthesized novel CeO₂-TG nanocatalyst is asC = 35.73%, O = 61.33%, and Ce = 2.94%. The EDX spectrum results show the purity of the created green nano-catalyst, which is recommended for the biodiesel production [31] and synthesized Pd nanocatalyst via green synthesis. The plant gum was used as a stabilizing agent. The results of EDX analysis confirmed the presence of Pd with other organic compounds. Akhtar et al. [13] analyzed the elemental composition of TG-modified NiSO₄ nanocatalyst. Carbon (C) peak was observed in the quantitative elemental analysis of the nano-catalyst synthesized, which is most likely due to the active ingredients in TG exudates used in the production and capping of the NPs. The current study's findings are comparable to those found in the literature.

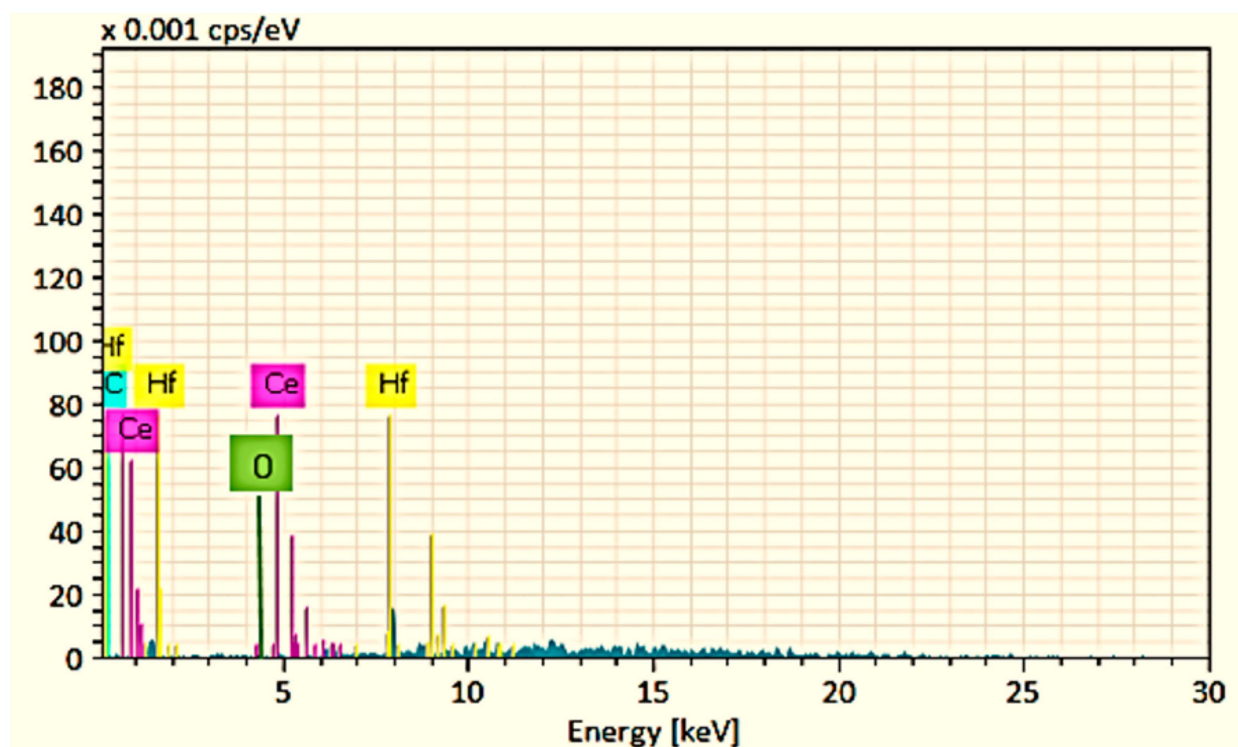


Figure 3. EDX analysis of TG-CeO₂.

3.2.3. Transmission Electron Microscopy (TEM)

The internal morphometry of synthesized TG-CeO₂ nanocatalyst is studied via TEM analysis (Figure 4) based on the electron transition from an image on a phosphorescent sheet. Light and dark areas in the image are associated with high density with less electron transition and low density with high electron transition, respectively [32]. The mean size of the particle nanocatalyst observed from the TEM image was 22 nm which matches the value reported by XRD analysis. The agglomeration of impregnated CeO₂ was observed on the TG support in different orders. The TG-CeO₂ nanoparticles exhibit a highly porous structure with a hexagonal shape and cylindrical walls. A porous structure with a large surface area can be assisted with a good stand for triglycerides molecule present in *D. sophia* oil to react with alcohol and produce biofuel [33] synthesized and characterized Ag nanoparticles from *Annona muricata* leaf extract. The findings showed spherical, mono-dispersed silver NPs with a mean particle of 22–28 nm. Sethy et al. [34] synthesized and characterized TiO₂ nanoparticles from *Syzygium cumini* via the green route. Results revealed that the crystal size matched the size determined via Debye Scherrer's equation in XRD analysis.

3.2.4. Thermogravimetric Analysis (TGA)

The effect of high temperature on the thermal stability of synthesized novel CeO₂-TG nano-catalyst was further analyzed via Thermogravimetric analysis (TGA). Figure 5 represents the TGA/DTA (Differential Thermal Analysis) curves of the CeO₂-TG nanocatalyst at two weight loss events. The curves were obtained in the nitrogen atmosphere at the intermediate rate of 10 °C/min. The thermal decomposition occurred from 400–450 °C with 3.8% weight loss due to water molecule (water of crystallization CeO₂·H₂O) evaporation. However, the thermal stability of the catalyst remained high up to 600 °C. After that, a minor weight loss confirmed moisture content elimination with organic residuals. It also proves the formation of support. Finally, significant weight loss occurs from 850–1050 °C due to the decomposition of the Cerium oxide (CeO₂) structure [35].

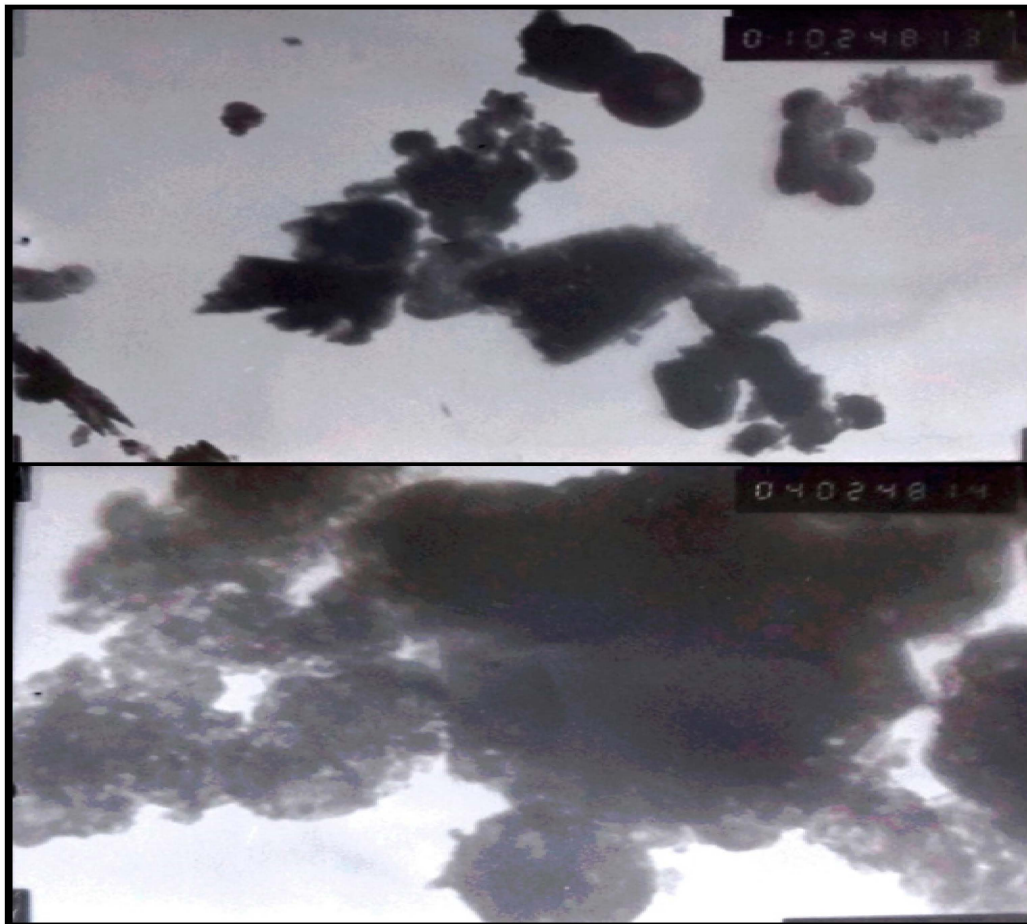


Figure 4. TEM micrographs of TG-CeO₂ at Different Resolutions.

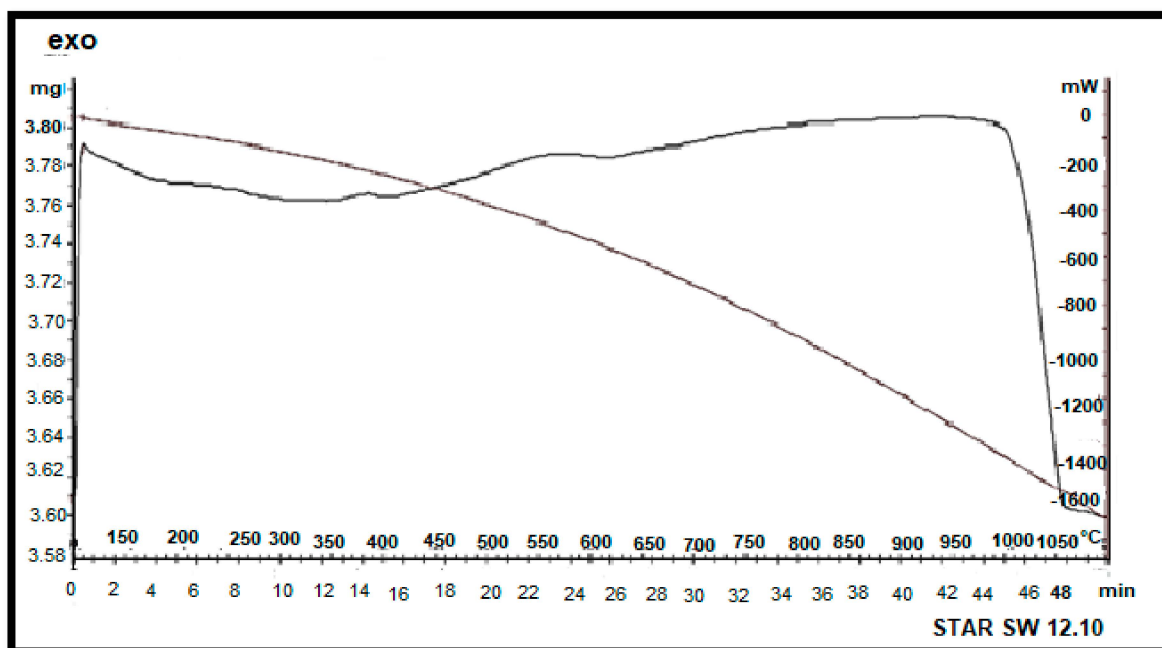


Figure 5. TGA/DTA plots of CeO₂-TG.

3.2.5. Functional Groups Analysis via FT-IR

The functional clusters present in the synthesized TG-CeO₂ nanocatalyst were analyzed via FT-IR spectra (Figure 6). The band appears at 540 cm⁻¹ showing the stretch vibration due to the Ce-O group. The stretching of the C-O bond was observed at 1183.51 cm⁻¹. A sharp, intense peak at 1379.47 cm⁻¹ was allocated to the deformation of the C-H bond. The characteristic asymmetric stretching vibration of -COO⁻ was observed at 1731.72 cm⁻¹, whereas the peak appeared at 2998.11 cm⁻¹ and was ascribed to the stretching vibration of the aliphatic -CH₃ group present in TG. The strong peak at 3520 cm⁻¹ corresponds to water-molecule stretching. Akhtar et al. [23] analyzed the efficiency of CuO-CeO₂ nanocatalyst for biofuel generation from *Sterculia feotida* seed oil. The characteristics peaks appeared at 681 and 690 cm⁻¹ revealing Cu-O particles. However, the peak visualized at 668 cm⁻¹ confirms the presence of CeO₂. The stretching of the O-H molecule was observed at 3648 cm⁻¹ and 3565 cm⁻¹. The FT-IR results of the current study are comparable to that of the previous research.

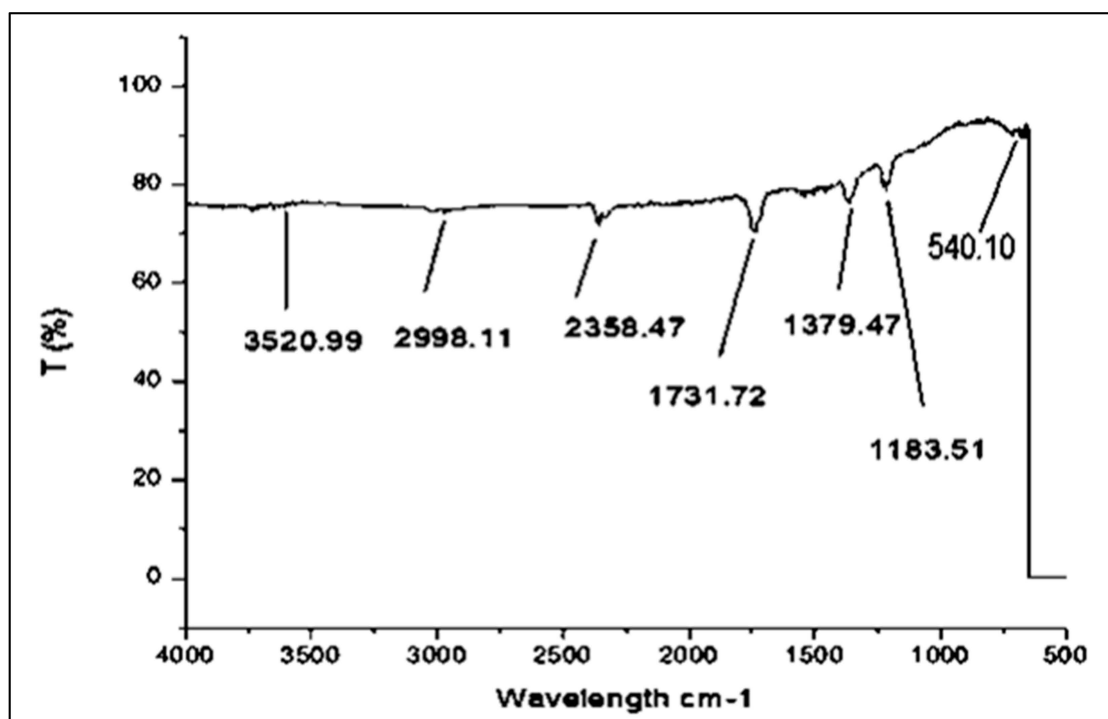


Figure 6. FTIR spectra of TG-CeO₂ nanocatalyst.

3.3. Model Validation and Optimization of DSBD via RSM-CCD

The effects of (A) catalyst concentration, (B) reaction temperature, (C) oil-to-methanol molar ratio, and (D) reaction duration on biodiesel yield (%) were investigated by varying their values from lower to higher (Table 1). Table 2 presents the analysis of variance (ANOVA) and regression coefficient. The regression model built from experimental data is depicted in Equation (5). The phrases' respective positive and negative indicators suggest complementary and opposing effects.

$$Y = +89.26 - 2.00A - 0.7222B + 5.06C - 1.67D - 2.25AB - 0.2500AC + 3.13AD + 0.1250BC - 3.75BD - 4.50CD - 6.86A^2 - 14.36B^2 - 8.36B^2 - 8.36C^2 - 11.86D^2$$

Predicted vs. actual biodiesel yield values are found adjacent to the straight line representing a good relationship between predicted and actual values (Figure 7). A high F-value (10.45) and a low *p*-value (<0.0001) is highly significant and also indicate the substantial effect of variables on the process yield [36]. The fact that the *p*-value for lack of

fit (0.70) was greater than 0.05 indicates that the model is appropriate for the experimental data. The adequate precision value (8.854) is greater than the minimum desired value of 4 [37], which shows the model's accuracy. $R^2 = 0.90$ showed that the approved polynomial equation determines more than 90% biodiesel production. Additionally, the adjusted $R^2 = 0.8203$ and predicted $R^2 = 0.6239$ have a slight difference of less than 0.2, confirming that the selected model is appropriate for examining the relationship among variables. The quadratic terms of the transesterification reaction, namely reaction temperature (B2) and reaction time (D2), have p -values of 0.05, indicating that they are significant, whereas catalyst concentration (A2) and methanol-to-oil molar ratio (C2) have p -values of >0.05 , indicating that they are insignificant.

Table 1. Experimental and predicted *D. sophia* yield using central composite design.

| Run | A: Catalyst Concentration | B: Reaction Temperature | C: Oil-to-Methanol Ratio | D: Reaction Time | Yield |
|-----|---------------------------|-------------------------|--------------------------|------------------|-------|
| | wt% | °C | | Min | % |
| 1 | 0.3 | 90 | 6 | 210 | 79 |
| 2 | 0.3 | 90 | 6 | 360 | 75 |
| 3 | 0.1 | 150 | 10 | 60 | 78 |
| 4 | 0.1 | 30 | 10 | 360 | 50 |
| 5 | 0.5 | 30 | 2 | 360 | 50 |
| 6 | 0.1 | 30 | 2 | 360 | 54 |
| 7 | 0.3 | 90 | 6 | 210 | 79 |
| 8 | 0.5 | 90 | 6 | 210 | 85 |
| 9 | 0.3 | 150 | 8 | 210 | 80 |
| 10 | 0.1 | 90 | 6 | 210 | 75 |
| 11 | 0.5 | 150 | 2 | 360 | 40 |
| 12 | 0.1 | 30 | 2 | 60 | 42 |
| 13 | 0.1 | 150 | 2 | 360 | 40 |
| 14 | 0.5 | 30 | 10 | 360 | 53 |
| 15 | 0.5 | 30 | 10 | 60 | 59 |
| 16 | 0.1 | 150 | 2 | 60 | 48 |
| 17 | 0.3 | 90 | 10 | 210 | 86 |
| 18 | 0.5 | 150 | 10 | 60 | 44 |
| 19 | 0.1 | 150 | 10 | 360 | 40 |
| 20 | 0.1 | 30 | 10 | 60 | 56 |
| 21 | 0.5 | 150 | 2 | 60 | 38 |
| 22 | 0.5 | 30 | 8 | 60 | 35 |
| 23 | 0.3 | 90 | 6 | 60 | 75 |
| 24 | 0.3 | 90 | 8 | 210 | 98 |
| 25 | 0.3 | 90 | 8 | 210 | 98 |
| 26 | 0.3 | 30 | 6 | 210 | 65 |
| 27 | 0.3 | 90 | 8 | 210 | 98 |
| 28 | 0.3 | 90 | 2 | 210 | 71 |
| 29 | 0.3 | 90 | 8 | 210 | 98 |
| 30 | 0.5 | 150 | 10 | 360 | 43 |

Table 2. Analysis of variance (ANNOVA) for Quadratic Model.

| Source | Sum of Squares | df | Mean Square | F-Value | p -Value | |
|--------------------------|----------------|----|-------------|---------|------------|-------------|
| Model | 11,235.74 | 14 | 802.55 | 10.45 | <0.0001 | Significant |
| A—Catalyst concentration | 72.00 | 1 | 72.00 | 0.9379 | 0.3482 | |
| B—Reaction Temperature | 9.39 | 1 | 9.39 | 0.1223 | 0.7314 | |
| C—Oil-to-methanol Ratio | 460.06 | 1 | 460.06 | 5.99 | 0.0271 | |

Table 2. Cont.

| Source | Sum of Squares | df | Mean Square | F-Value | p-Value | |
|-----------------|----------------|----|--------------------------|---------|---------|-----------------|
| D—Reaction time | 50.00 | 1 | 50.00 | 0.6513 | 0.4322 | |
| AB | 81.00 | 1 | 81.00 | 1.06 | 0.3206 | |
| AC | 1.0000 | 1 | 1.0000 | 0.0130 | 0.9106 | |
| AD | 156.25 | 1 | 156.25 | 2.04 | 0.1742 | |
| BC | 0.2500 | 1 | 0.2500 | 0.0033 | 0.9552 | |
| BD | 225.00 | 1 | 225.00 | 2.93 | 0.1075 | |
| CD | 324.00 | 1 | 324.00 | 4.22 | 0.0578 | |
| A ² | 121.91 | 1 | 121.91 | 1.59 | 0.2268 | |
| B ² | 534.24 | 1 | 534.24 | 6.96 | 0.0186 | |
| C ² | 181.06 | 1 | 181.06 | 2.36 | 0.1454 | |
| D ² | 364.41 | 1 | 364.41 | 4.75 | 0.0457 | |
| Residual | 1151.46 | 15 | 76.76 | | | |
| Lack of Fit | 670.13 | 10 | 67.01 | 0.6961 | 0.7079 | not significant |
| Pure Error | 481.33 | 5 | 96.27 | | | |
| Cor Total | 12,387.20 | 29 | R ² | 0.9070 | | |
| Std. Dev | 8.76 | | Adjusted R ² | 0.8203 | | |
| C.V. % | 13.60 | | Predicted R ² | 0.6239 | | |
| | | | Adeq Precision | 8.8543 | | |

Key: df = degree of freedom, C.V = coefficient of variation, Std. Dev = standard deviation.

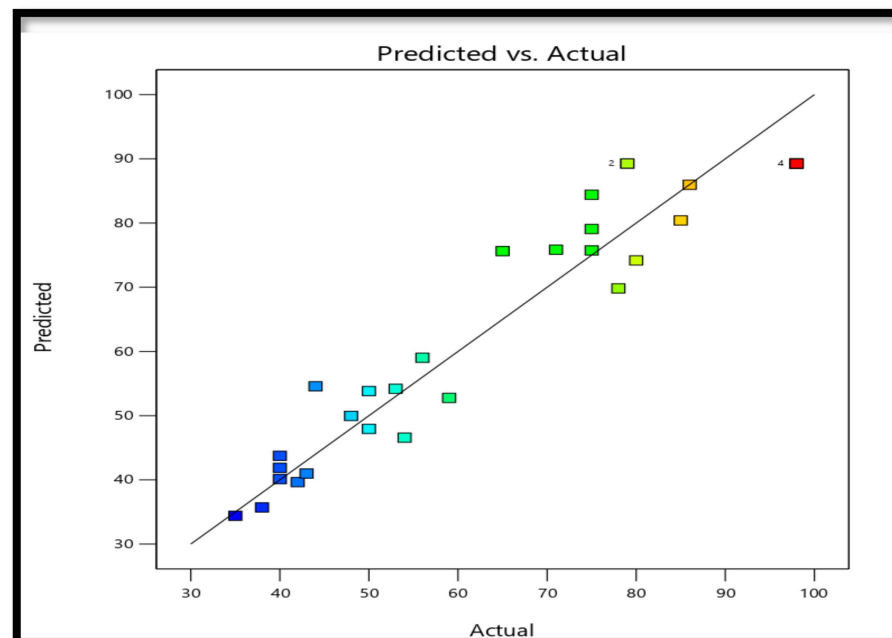


Figure 7. Predicted vs. actual biodiesel yield of *D. sophia* biodiesel.

3.4. Reaction Parameters Consequence on Biodiesel Yield

3.4.1. Combined Effect of Catalyst Concentration and Reaction Temperature

The catalyst concentration and the reaction temperature impact the biodiesel yield during the transesterification reaction. When the molar ratio of oil to methanol and

the reaction time were held constant, Figure 8A shows the combined effect of catalyst concentration and reaction temperature on biodiesel yield (%). It appears that increasing reaction temperature and catalyst concentration results in an increase in biodiesel yield up to a certain degree. It has been found that when the reaction temperature climbed from 30 °C to 90 °C, the biodiesel conversion (%) increased with an increase in catalyst concentration in the range of roughly 0.1 wt% to 0.3 wt%. It accelerates the transesterification process by reducing activation energy and increasing molecular collision rate, which boosts the final biodiesel yield [38]. Table 1 shows that maximum biodiesel yield (98%) was attained with (0.3 wt%) catalyst concentration and 90 °C temperature. However, an abrupt decline in biodiesel yield of 56% was observed at 30 °C temperature and catalyst concentration 0.1 wt%. Similar trends were seen with a 38% biodiesel production at the maximal catalyst concentration (0.5 wt%) and reaction temperature (150 °C). High temperature and catalyst concentration favors the reversible reaction due to the saponification of triglycerides and decrease the biodiesel yield. These findings concur with the study of [13,39]. With a p -value of $0.32 > 0.05$, ANOVA results were determined to be insignificant in this study.

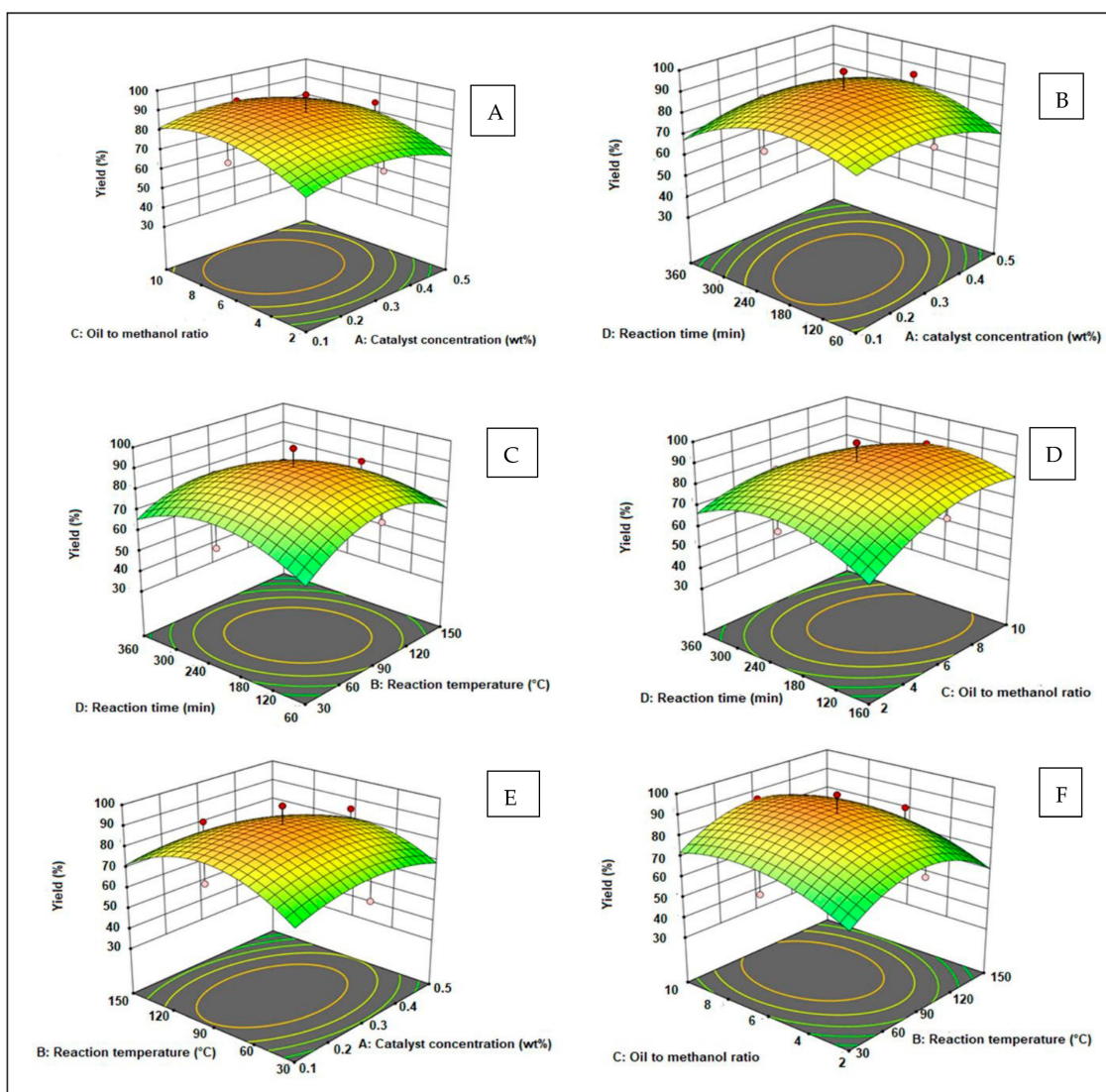


Figure 8. The 3D plots (A–F) present the impact of different optimization parameters on *D. sophia* biodiesel yield.

3.4.2. Combined Effect of Catalyst Concentration and the Molar Ratio of Oil to Methanol

The combined effect of catalyst concentration and the oil-to-methanol ratio has been given at constant temperature and reaction time (Figure 8B). Catalyst concentration and the molar ratio of oil to methanol significantly impact biodiesel yield. It was discovered that raising the catalyst concentration from 0.1% to 0.3% and the methanol to oil molar ratio from 1:2 to 1:8 enhanced the biodiesel yield (%). Maximum biodiesel yield (98%) was obtained at 0.3 wt% catalyst concentration and 1:8 oil-to-methanol ratio. An adequate quantity of CH₃OH is necessary for the transesterification reaction to transform the triglycerides into biodiesel. The regression curve was seen as the oil-to-methanol ratio decreased and the amount of biodiesel produced decreased. However, excessive methanol in the transesterification process results in an emulsified mixture with products, making the biodiesel separation process more difficult. This demonstrates that, compared to other parameters, the oil-to-methanol ratio has the greatest impact on the transesterification process for biodiesel conversion. Because it impacts catalytic activity, catalyst concentration is crucial to biodiesel output. A decline in biodiesel yield of 35% was observed at 0.5 wt% catalyst concentration, while the oil-to-methanol ratio remained the same (1:8). This decrease is due to a weaker contact between catalytic reactive sites and triglyceride molecules. The highly viscous reaction mixture is another cause of biodiesel yield decline with excess catalyst concentration [40]. With a *p*-value of 0.91 (>0.05), these parameters' collective impact is insignificant. These findings are comparable with the literature study [38].

3.4.3. Combined Effect of Catalyst Concentration and Reaction Time

The combined impact of catalyst concentration and reaction time on biodiesel yield at constant oil-to-methanol ratio and reaction time is depicted by a 3D response surface plot (Figure 8C). Due to equilibrium, the highest biodiesel conversion (98%) was attained at a reaction time of 210 min and catalyst concentration of 0.3 wt% (Run 24). The greatest biodiesel production was 43% at a maximum catalyst concentration of 0.5 wt% and a reaction period of 360 min (Run 30). Excess catalysts increase the mass transfer resistance in the trans-esterification reaction, resulting in a slow diffusion rate of triglycerides, methanol, and catalyst. It was also discovered that the short reaction time and highest catalyst concentration result in a low biodiesel yield (35%) (Run 22). Therefore, the long reaction time (360 min) for the transesterification process favors the reversible reaction and reduces the biodiesel yield (40%) (Run 19). The proper catalyst dosage, which contains high acidity and particular surface areas that improve the catalyst's acidic strength, is widely recognized to play an essential role in the biodiesel synthesis [41]. The combined influence of catalyst concentration and reaction time with *p*-value (0.1742) > 0.05 was insignificant.

3.4.4. Combined Effect of Reaction Temperature and the Molar Ratio of Oil to Methanol

Figure 8D depicts the combined effect of reaction temperature and the molar ratio of oil to methanol on biodiesel yield (%), while other parameters are at the center point. Biodiesel yield increases up to 98% at 90 °C temperature and 1:8 oil-to-methanol ratio, which is attributed to the maximum interaction of triglycerides and methanol during the transesterification process. According to the Arrhenius equation, the chemical reaction and methyl ester yield steadily increase as the reaction temperature rises [42]. However, as short reaction temperature (30 °C) and a low oil-to-methanol ratio (1:6) ensued, there was a decrease in biodiesel yield (65%) (Run 26) which is more certain at lower temperatures, and the mass transfer rate of reactants became decreased due to immiscibility [13]. The sudden drop in biodiesel yield (40%) was observed at the highest temperature of 150 °C and the oil-to-methanol ratio of 1:10 (Run 19) due to volatilization of methanol at high temperatures. Similar results were reported in previous studies [23]. ANOVA results showed that the combined influence of these variables is insignificant by having a *p*-value of (0.95) > 0.05.

3.4.5. Combined Effect of Reaction Temperature and Reaction Time

The combined effect of reaction temperature and duration on transesterification is depicted in Figure 8E. At 90 °C and 210 min reaction time, there was a significant increase in biodiesel output (98%). The decrease in biodiesel yield was experienced as the temperature and time over the threshold value increased. Higher temperatures and reaction periods are expected to speed up the chemical process of turning alkyl esters into acids. The biodiesel yield is decreasing due to the subsequent polar methanol in the reaction mixture, whereas partial conversion of triglycerides into biodiesel (42%) was observed at 30 °C for 60 min (Run 12) [43]. With a p -value (0.10) > 0.05, the ANOVA results showed that the combined effect of reaction temperature and duration was not significant.

3.4.6. Combined Effect of Molar Ratio of Oil to Methanol and Reaction Time

The reaction time and oil-to-methanol molar ratio are the most important factors that affect biodiesel yield. A 3D figure depicting the combined impact of oil to methanol molar ratio and reaction time on *D. sophia* biodiesel yield was created (Figure 8F), with the remaining two parameters at the center point. For the biodiesel yield to rise, further methanol is needed. In this investigation, the greatest biodiesel output (98%) was achieved at an oil-to-methanol ratio of 1:8 and a reaction period of 210 min (Run 24). It was observed that high methanol content could convert triglycerides into monoglycerides during the transesterification reaction. However, after a certain limit, further addition of methanol content makes separating biodiesel from glycerol difficult and substantially decreases the biodiesel yield [44,45], whereas a shorter reaction time of 60 min with a low molar ratio of oil to methanol 1:2 leads to (38%) biodiesel yield (Run 21). It is most likely due to a lack of time for reactants to react properly, resulting in the incomplete conversion of reactants into products. The biodiesel yield was reduced by 86% at a higher oil-to-methanol ratio of 1:10 for 210 min (Run 17) due to a reverse reaction, which decreased the biodiesel yield. These results were comparable with the previous literature [46]. ANOVA results showed that the combined effect of these two parameters was significant, with a p -value of 0.05.

3.5. *D. sophia* (L.) Biodiesel Characterization

3.5.1. FT-IR Spectroscopy Study of Biodiesel

It is an efficient analytical technique that uses fingerprinting to identify the chemical bonds and functional groups in oil and biodiesel [47]. FTIR spectrum of *D. sophia* seed oil and *D. sophia* biodiesel product have similar chemical structures. However, they have small differences in intensities and frequencies of the absorption band [48]. In (Figure 9A), the broader peaks were observed at $\sim 3465.44\text{--}2890.26\text{ cm}^{-1}$ in oil spectra, while biodiesel spectra (Figure 9B) showed strong stretching of the C-H methoxy group. Additionally, *D. sophia* seed oil has only a single peak at 1450.68 cm^{-1} attributed to asymmetric (C-H) deformation, while in *D. sophia* biodiesel spectra (Figure 9B), peaks were observed at 1456.67 cm^{-1} and 1436.87 cm^{-1} representing asymmetric bending of CH_2 and asymmetric stretching of CH_3 , respectively. An observable characteristic peak in both spectra of oil and biodiesel at 1742.02 cm^{-1} is attributed to a carbonyl group (C=O) stretching, which confirms the presence of an ester compound. In the IR spectrum of Brassica juncea biodiesel, the peak of the carbonyl group was observed at 1744 cm^{-1} [13]. However, it was discovered at 1740 cm^{-1} in the biodiesel from *Celastrus paniculatus* [49]. These results are in line with the present study. The fingerprint region from $1500\text{--}900\text{ cm}^{-1}$ illustrates the difference between the oil and biodiesel spectrum. A strong peak observed at 1145.87 cm^{-1} (Figure 9A) fragmented into two peaks, i.e., 1130.32 cm^{-1} and 1118.67 cm^{-1} . A peak at 964.35 cm^{-1} relates to CH_2 wagging for oil absent in biodiesel. Strong stretching of the alkane group appeared at 580.56 cm^{-1} [50]. FTIR results showed that *D. sophia* seed oil was effectively converted into *D. sophia* biodiesel.

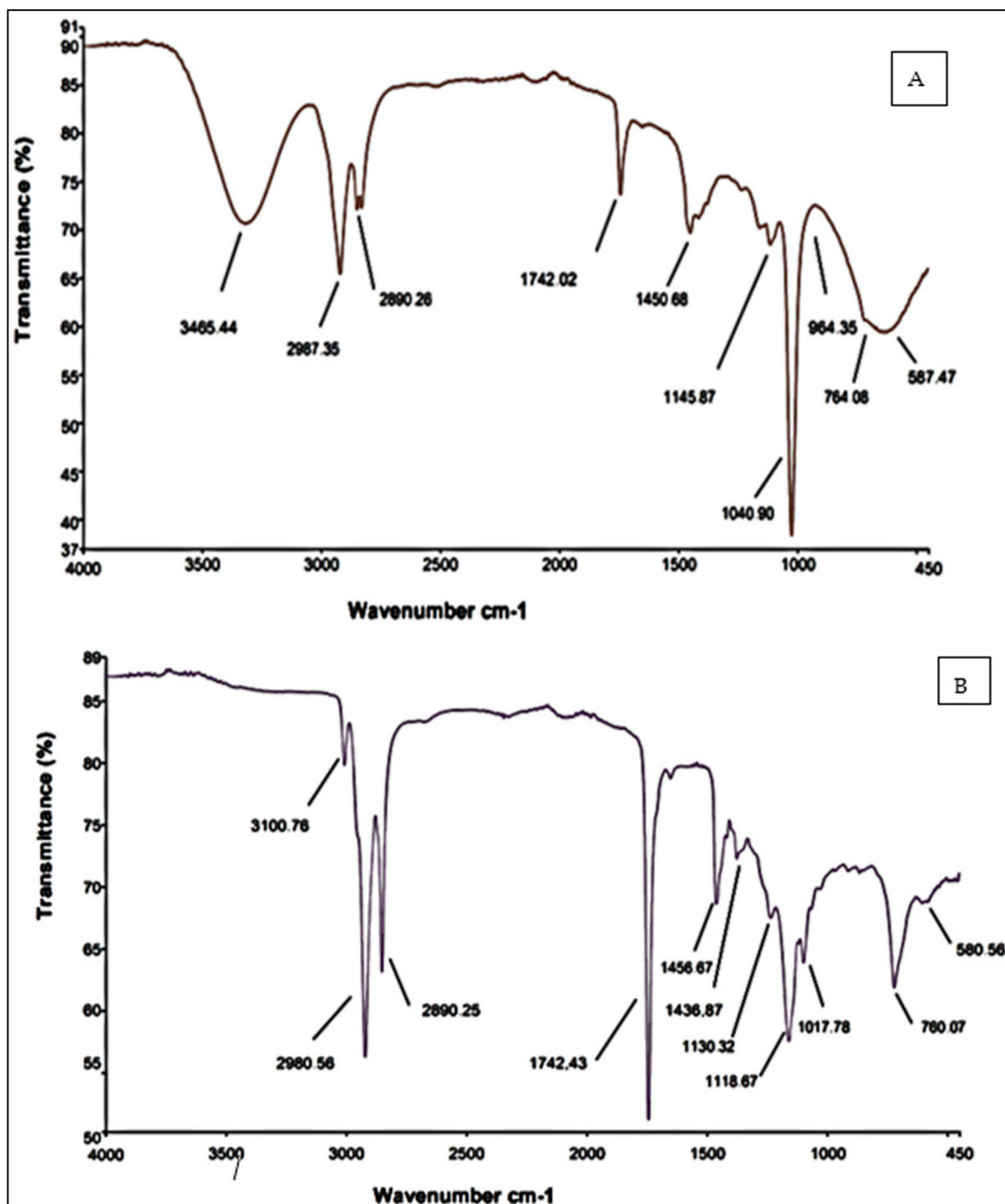


Figure 9. FT-IR spectrum of (A) *Descurainia sophia* Webb ex Prantl. Seed oil; (B) *Descurainia sophia* Webb ex Prantl. Biodiesel.

3.5.2. GCMS Analysis of Biodiesel

The variations in the chemical composition of biodiesel are thought to have a substantial impact on its chemical and physical qualities. Therefore, the chemical composition of FAMES was analyzed using gas chromatography and mass spectroscopy to assess the biodiesel's quality. The GCMS spectra of BJBBD (Figure 10) show several FAME peaks further recognized via Library match software (No. NIST 11). The retention duration of the various FAMES was utilized to identify them, and MS analysis was used to confirm

them [51]. The 11-Octadecanoic acid methyl ester, 11-Eicosenoic acid methyl ester, Pentadecanoic acid methyl ester, Hexadecanoic acid methyl ester, Heptadecanoic acid methyl ester, Docosanoic acid methyl ester, and Tetracosanoic acid methyl ester are the main fragments in the characteristic mass spectrum of 9, 12-Octade. The basic peak of the fatty acid methyl ester was discovered at 55 m/z .

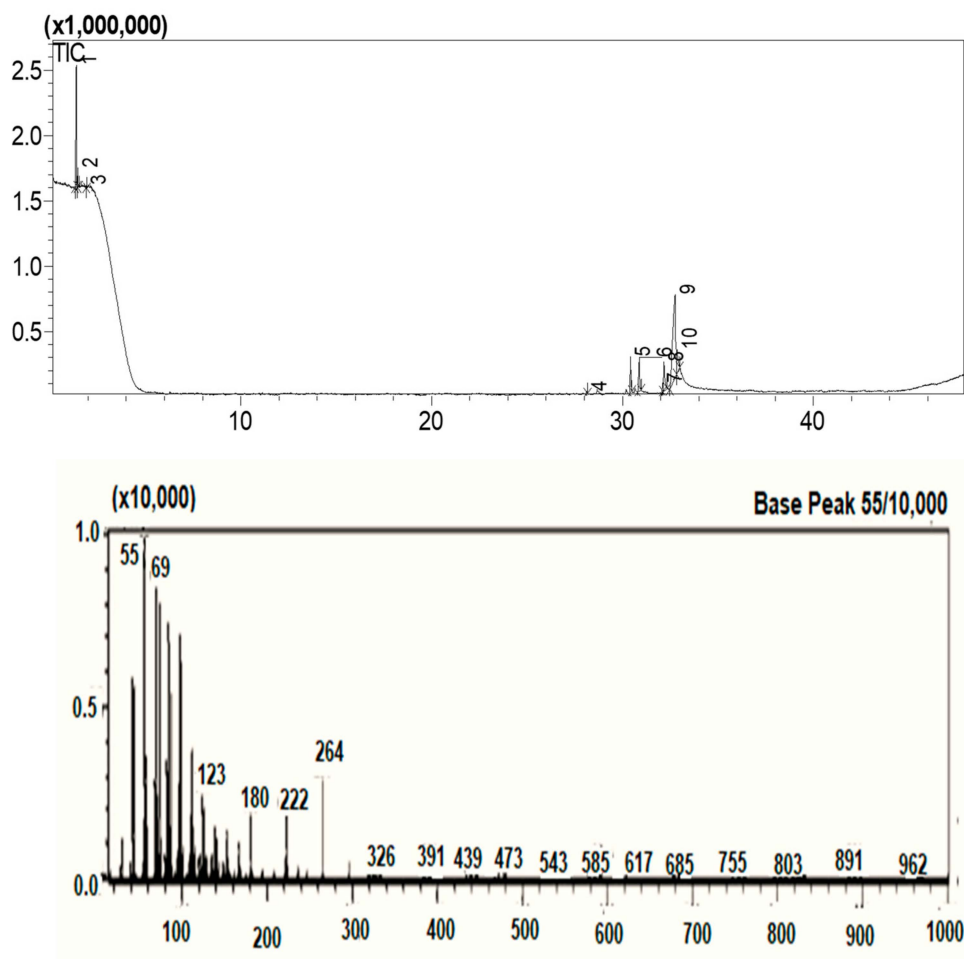


Figure 10. GCMS spectra of *D. sophia* biodiesel (**upper**); library match (**lower**).

3.5.3. NMR Analysis of Biodiesel

D. sophia biodiesel was further analyzed via NMR (^1H and ^{13}C). The molecular makeup of biodiesel was ascertained using the ^1H NMR method, which was also used to confirm that methyl ester was synthesized during the transesterification reaction. Figure 11 (upper) illustrates the ^1H NMR spectrum of biodiesel and its respective signals. The signals appeared at 0.88 ppm, attributed to terminal methyl protons (C-CH₃) at 1.23–1.67 ppm, and at 2.01 ppm, they were attributed to methylene group (α -CH₂, β -CH₂), which denoted the presence of hydrogen atoms on the third carbon in an aliphatic fatty chain. The peak at 0.87 ppm corresponded to the terminal methyl protons, while the peak for olefinic hydrogen (-CH=CH-) displayed the double bond integrated for two hydrogen atoms for each double bond group, which was seen at 5.32 ppm. Allylic hydrogen (-CH₂), which has two hydrogen atoms per non-conjugated group in the spectrum, exhibits a peak at 2.76 ppm. The appearance of a characteristic single peak at 3.5 ppm attributed to methoxy protons (-OCH₃) confirms the synthesis of methyl esters. The ^{13}C NMR spectra (Figure 11 (lower)) indicate characteristic signals at 30.11 ppm, and 174.21 ppm corresponds to (-CH₂)_n and (-COO-), respectively. The unsaturated position in a DSBD (CH=CH) methyl ester was observed at 127.8 ppm for inner non-conjugated carbon. The chemical shifts observed

at δ (ppm): 29.35 ($-\text{CH}_2-$)_n, 77.5 ($-\text{C}-\text{O}$), 129.8 ($-\text{CH}=\text{CH}-$); outer non-conjugated carbon was observed in the biodiesel spectrum [13]. All these peaks are similar to earlier described work [52,53]. The total conversion of *D. sophia* oil into biodiesel was 99% by employing the formula given by [43], which is very close to the practically obtained biodiesel yield (98%).

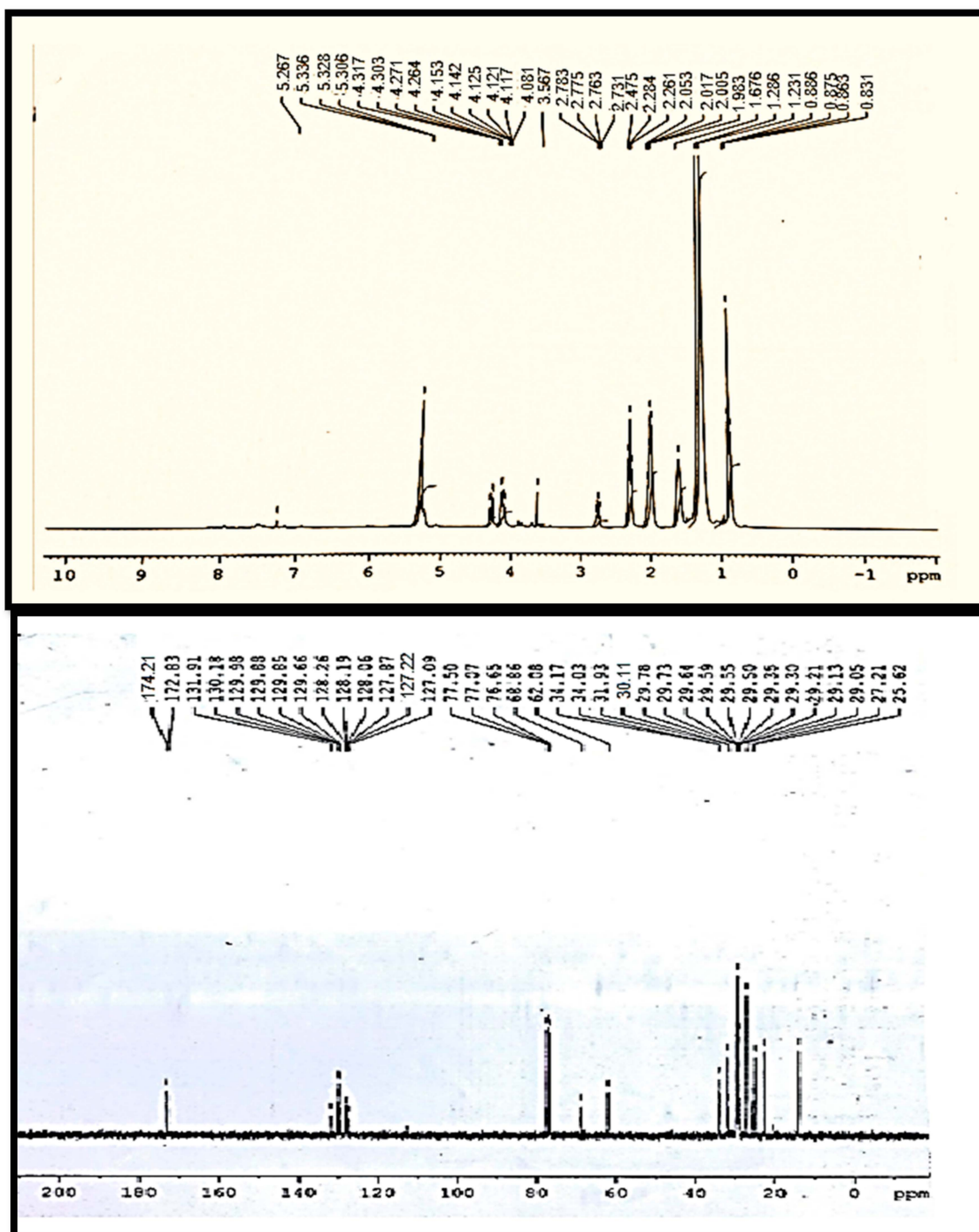


Figure 11. NMR Spectra of *D. sophia* biodiesel ^1H (upper), ^{13}C (lower).

3.6. Fuel Properties of *D. sophia* Biodiesel in Comparison with International Standards

Fuel properties of synthesized *D. sophia* biodiesel were investigated before its application in a diesel engine. The properties of biodiesel fuel vary depending on the feedstock and are determined mainly by the fatty acid composition of the oil [14]. The fuel qualities

of *D. sophia* biodiesel and their comparison with worldwide biodiesel standards, such as (ASTM D-6751, 951), (EN-14214), and China (GB/T 20828). Table 3 shows the similarity of the fuel properties of *D. sophia* biodiesel (DSBD) with those of the abovementioned international biodiesel standards. It is essential to determine the fuel's properties to know its characteristics and usefulness for diesel engines before its practical use on a larger scale. According to ASTM standards, the color of *D. sophia* biodiesel is visual 2.5.

Table 3. Comparison of fuel properties of *D. sophia* biodiesel with international standards.

| Properties | Methods | Current Study | HSD ASTM D-951 | ASTM D-6751 | EN-14214 | China GB/T 20828-2007 |
|----------------------------|-------------|---------------|-------------------|-------------|----------|--------------------------|
| Color | Visual | 2 | 2.0 | 2 | - | - |
| Flashpoint °C (PMCC) | ASTM D-93 | 73.5 | 60–80 | ≥93 | ≥120 | ≥130 |
| Density@ 15 °C kg/L | ASTM D-1298 | 0.800 | 0.8343 | ≤120 | ≤120 | - |
| K. Viscosity@40 °C cSt | ASTM D-445 | 4.23 | 4.223 | 1.9–6.0 | 3.4–5.0 | - |
| Pour point °C | ASTM D-97 | −7 | - | −15–16 | - | - |
| Cloud point °C | ASTM D-2500 | −12 | - | −3–12 | - | - |
| Sulfur %wt | ASTM D-4294 | 0.0001 | 0.05 | ≤0.05 | 0.020 | ≤0.05 |
| Total Acid No.mg KOH/gm | ASTM D-974 | 0.160 | 0.8 | ≤0.5 | ≤0.5 | ≤0.8 |

Kinematic viscosity is a crucial factor that affects fuel injection, atomization, and fuel sprays in terms of the characteristics of biodiesel fuel [54]. Biodiesel fuel viscosity is 10–15 times higher than petro-diesel due to cyclic compounds, which impact the engine's fluid volume and injection characteristics [55]. In the present study, the measured kinematic viscosity of *D. sophia* (L.) is 4.23 mm²/s which was compatible with ASTM D-951 (4.22), ASTM D-6751 (1.9–6.0), and EN 14214 (3.4–5.0) (Table 3). Kinematic viscosity in the present study (4.23 mm²s) is significantly lower than *Brassica juncea* (4.66 mm²s) [13], *Jatropha* (4.30 mm²s), and Palm (4.50 mm²s), but is in line with the international standards [56].

Another significant fuel characteristic is the acid number that adversely affects engine efficiency and is directly related to the amount of FFA in diesel fuel [13,23]. If more FFA exists, the acid number will increase, directly affecting other attributes due to their higher melting points [57]. The acid content of *D. sophia* biodiesel is (0.160 mg KOH/g), which is significantly lower than the acid content of *A. julibrissin* biodiesel (0.2 mg KOH/g) [58].

The flash point is the lowest temperature at which gasoline ignites. Biodiesels with low flash points are more flammable than those with high flash points, which ultimately causes carbon buildup in the diesel engine's combustion chamber. Fuels, having higher flash points (>66 °C), provide safety during transport and handling (Esmaili and Foroutan, 2018) and are declared safe for diesel engines [59]. *D. sophia* biodiesel has a flash point of 73.5 °C, greater than *Citrus aurantium* biodiesel, which has a flash point of 71 °C [60].

The temperature at which biodiesel flows the least is known as its pour point [23]. This is because the percentage of saturated fatty acids in biodiesel grows, and so does the pour point. At the same time, the cloud point is the temperature above 0 °C, at which wax crystal formation occurs. The recorded value of the pour point and cloud point of *D. sophia* (L.) biodiesel is −7 °C and −12 °C, which matched international standards.

The efficiency of fuel atomization depends on biodiesel density and is directly linked to the fuel quality and purity [55]. The density of biodiesel is improved by having the longest chain length and maximum oil-saturation level. Like gasoline, biodiesel has a greater impact on diesel engine efficiency due to its higher density. The recorded density of *D. sophia* (L.) biodiesel was (0.800 kg/m³ at 40 °C), which was close to the international biodiesel standards (Table 3), which assures that its use in diesel engines has no adverse effects on the environment or engine performance [61].

D. sophia biodiesel has a sulfur concentration of 0.0001%wt, which lies within the prescribed international limits. Biodiesel with low sulfur level (<1 ppm) has been deemed environmentally benign and pollution-free, making it appropriate for use at the commercial level [62].

3.7. Catalyst Reusability

Reusability is one of the most important factors to consider when evaluating catalyst performance. The catalyst's durability and practicality for producing biodiesel on an industrial scale depend on its capacity for recycling in a reaction process. The nature and kind of the catalyst and the purification, separation, and transesterification procedure impact the reusability of the nanocatalysts [56]. The nanocatalyst can be easily detached from the product and recycled at the end of the reaction in the present study. The reusability of TG-CeO₂ was studied at optimized reaction conditions, i.e., the molar ratio of oil to methanol (1:8) and catalyst concentration (0.3 wt%) at 90 °C for 210 min. After each reaction round, the used catalyst was washed multiple times with CH₃OH, oven-dried at 60 °C for 4 h, and reused in the next reaction. The reused catalyst showed a drop in performance in the second round (2%) and the third round (8%) (Figure 12). The best catalyst can provide biodiesel yield (80%) through the third round, according to the results of the catalyst reusability test. However, in the fourth round, there was a decline in catalytic activity as a result of the catalyst's basicity, small surface area, leaching from organic species, such as glycerol, and deactivation of the active sites on the catalyst [60].

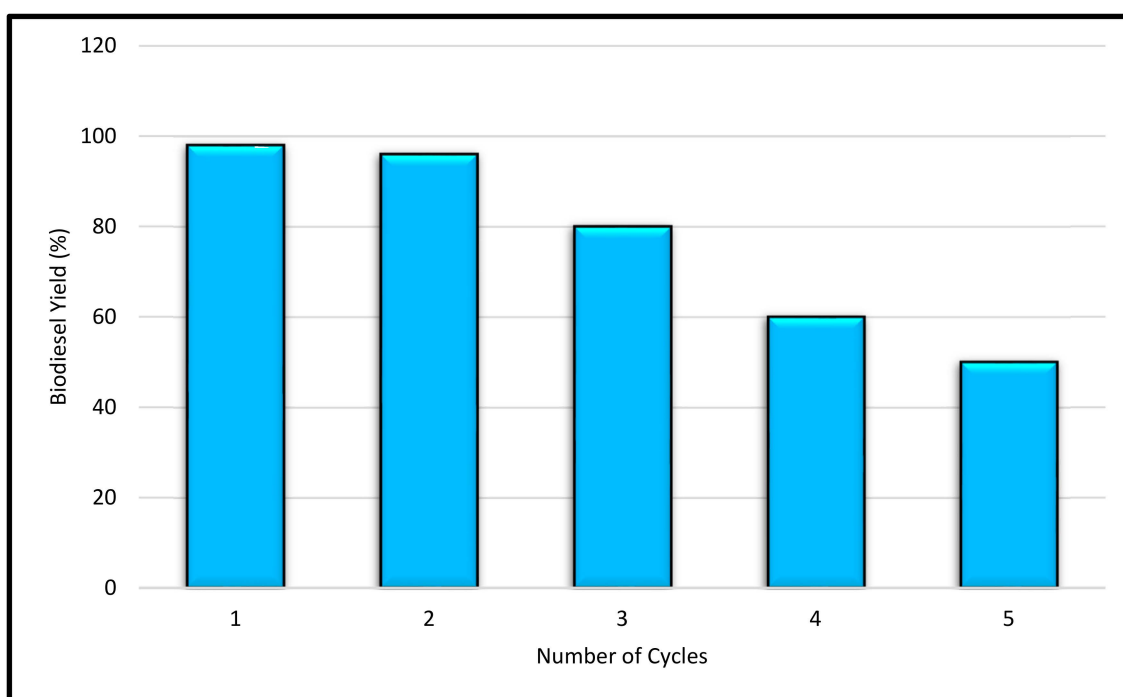


Figure 12. TG-CeO₂ phytonanocatalyst reusability analysis at optimized reaction parameters.

3.8. Limitations and Future Aspects of the Present Study

The desire to decrease the effects of growing energy consumption, environmental concerns, and resource depletion are the primary reasons for using alternative energy sources. The substantial study on biodiesel has greatly benefited the biofuel market. Various feedstocks can be used for biodiesel synthesis, including edible and non-edible vegetable oils, waste biomass oil, algal oil, animal fat oil, etc. However, several significant issues require specific consideration, including production cost, food security, and water intensiveness, to make the biofuel market more competitive worldwide [56,63]. Additionally, efforts should

be made to identify and explore the potential of non-edible, poisonous, and wild oil seeds as effective feedstock for affordable and environment-friendly biodiesel production.

Biofuels, the preferable biodiesel, are synthesized via transesterification reaction with a catalyst. However, catalyst properties and performance depend on the nature of the catalytic material utilized, reaction conditions, and the post-separation process. In this context, nanotechnology is crucial for strategizing and creating highly-skilled, cost-effective, and eco-friendly phyto nanocatalysts that might support the synthesis of high-quality and cost-effective biodiesel [64]. As a result, a brand-new TG-CeO₂ phytonanocatalyst that is thermally stable, economical, eco-friendly, reusable, and contains the highest possible catalytic activity during reaction has been used in the current research. Future research should be devoted to plant extract-based nanocatalyst synthesis, focusing on the use of vegetable wastes because they contain the same organic agent as raw materials and may, thus, close the sustainability loop. Additionally, contemporary and updated statistical tools, such as artificial neural networks (ANN), could be used to forecast the optimal biodiesel yield based on the experimental output.

The circular economy concept provides a wide lens to sustain the environmental production–consumption system, combat the pressures of economic expansion, and enhance ecological functioning and human well-being [65]. In order to build a sustainable future, investments in the area where the circular economy and bio-economy intersect have become more popular. The circular economy's preconditions include optimal production, consumption, and circular flow valorization to ensure sustainability standards. It promotes resource efficiency and the idea of zero waste, which could be very helpful in reaching the Sustainable Development Goals (SDGs-2030). The circular economy has recently been developing and linking cleaner manufacturing ideas to lengthen the period that materials and energy circulate inside each system, saving virgin materials and energy while also drawing attention to the flow of biomaterials and their potential for recovery.

Resilience is keeping a system inside its current basin without crossing over to a different basin [66]. Resilience has been considered a prerequisite for sustainability even though this concept is still developing and unclear, particularly in certain industries, such as the energy industry. Savings in materials, energy, and waste help to promote sustainability and resilience by protecting natural resources and lowering emissions [67]. The present concept of resilience emphasizes coupled socio-ecological systems' capacity to withstand change and upheaval, adapt to impending challenges, and transform in ways that maintain the ability to function and provide ecosystem services [68]. Resilience is also more appropriate for today's energy policy framework [69]. The generation of waste, the energy issue, the water crisis, and pollution challenges are only a few of the disparate concepts connected to creating a resilient and sustainable circular economy. There is a need to integrate the theory of resilience with energy and provide possible solutions to apply resilience to energy systems to answer questions, such as duration of disruption and time of action, which still have to be addressed.

4. Conclusions

Researchers are presently examining renewable energy sources, such as biodiesel, due to their potential to battle energy deficit and environmental deterioration. This is due to the current energy crisis and the rapidly diminishing fossil fuel reserves. Non-edible seed oils have become well-known among researchers because of their accessibility, biodegradability, and practicability. Biofuel technology is a viable, cost-effective, and efficient alternative to traditional fossil fuels in the commercial sector. The present study is designed to examine the potential of novel and non-edible *D. sophia* with 36% (*w/w*) seed oil content for synthesizing biodiesel using newly synthesized and biodegradable phytonanocatalyst of TG-modified CeO₂. The FFA content of seed oil was less than 3% and favored single-step transesterification. The newly synthesized phytonanocatalyst TG-CeO₂ exhibited significant catalytic properties during converting triglycerides into biodiesel. The maximum biodiesel yield (98%) was postulated at a 1:8 molar ratio of oil to methanol,

0.3 wt% catalyst amount at 90 °C, and 210 min reaction time. The optimized parameters and their interaction effects on final biodiesel yield were studied using the updated statistical technique, i.e., RSM coupled with CCD *p*-value and R^2 0.9070, which indicates the model's suitability in predicting design space for the biodiesel yield. TLC, FT-IR, and NMR methods were used to confirm the synthesis of FAME in a biodiesel sample.

In contrast, the chemical composition of *D. sophia* biodiesel was examined using GCMS analysis. Catalyst reusability under optimized reaction conditions was consistent up to the third cycle with 80% biodiesel yield. Biodiesel fuel properties were in excellent agreement with international biodiesel standards, denoting it as a suitable feedstock for biodiesel synthesis. The importance of this research in utilizing inexpensive, non-edible feedstock and the implication of synthesized novel phytonanocatalyst using a simple method and excellent fuel properties of synthesized biodiesel provides a suitable perspective for its resilience at the industry level for effectual and commercial production of biodiesel from waste resources. However, further research is required to determine the *D. sophia* biodiesel effects on engine performance and emissions of gasses. It is also recommended to study the life-cycle assessment (LCA) of *D. sophia* seed oil and determine the benefits of this unique feedstock in terms of socioeconomics, technology, and the environment.

Author Contributions: M.T.A.: collected the seeds, performed the whole experiment, and prepared the first original draft; M.A. (Mushtaq Ahmad): supervision, conceptualization, visualization; M.A. (Maliha Asma): investigation, methodology; M.Z.: writing—review and editing; M.F.R.: data curation, reviewing and editing; T.M.: methodology; A.Y.: visualization; O.M.: statistical analysis; M.M.: writing, reviewing, and editing; S.M.: writing, reviewing, and editing. All authors have read and agreed to the published version of the manuscript.

Funding: Deanship of Scientific Research at Umm Al-Qura University, Grant Code: 23UQU4430043DSR002.

Institutional Review Board Statement: Not applicable.

Informed Consent Statement: Not applicable.

Data Availability Statement: Not applicable.

Acknowledgments: The authors would also like to thank the Deanship of Scientific Research at Umm Al-Qura University for supporting this work by Grant Code: 23UQU4430043DSR002. Trobjon Makhkamov would like to thank the Ministry of Innovative Development of the Republic of Uzbekistan (Project no. AL 2021090820).

Conflicts of Interest: The authors declare that they have no known competing financial interests or personal relationships that could have appeared to influence the work reported in this paper.

References

1. Chozhavendhan, S.; Singh, M.V.P.; Fransila, B.; Kumar, R.P.; Devi, G.K. A review on influencing parameters of biodiesel production and purification processes. *Curr. Res. Green Sustain. Chem.* **2020**, *1*, 1–6. [[CrossRef](#)]
2. Suresh, T.; Sivarajasekar, N.; Balasubramani, K. Enhanced ultrasonic assisted biodiesel production from meat industry waste (pig tallow) using green copper oxide nanocatalyst: Comparison of response surface and neural network modelling. *Renew. Energy* **2021**, *164*, 897–907. [[CrossRef](#)]
3. Noshadi, I.; Amin, N.; Parnas, R.S. Continuous production of biodiesel from waste cooking oil in a reactive distillation column catalyzed by solid heteropolyacid: Optimization using response surface methodology (RSM). *Fuel* **2012**, *94*, 156–164. [[CrossRef](#)]
4. Khan, I.W.; Naeem, A.; Farooq, M.; Ghazi, Z.A.; Saeed, T.; Perveen, F.; Malik, T. Biodiesel production by valorizing waste non-edible wild olive oil using heterogeneous base catalyst: Process optimization and cost estimation. *Fuel* **2022**, *320*, 123828. [[CrossRef](#)]
5. Anwar, M.; Rasul, M.G.; Ashwath, N.; Nabi, M.N. The potential of utilizing papaya seed oil and stone fruit kernel oil as non-edible feedstock for biodiesel production in Australia—A review. *Energy Rep.* **2019**, *5*, 280–297. [[CrossRef](#)]
6. Cheema, S.I.; Ahmad, M.; Ullah, R.; Mothana, R.A.; Noman, O.M.; Zafar, M.; Sultana, S.; Hameed, A.; Naz, S.; Akhtar, M.T. Implication, visualization, and characterization through scanning electron microscopy as a tool to identify nonedible oil seeds. *Microsc. Res. Tech.* **2021**, *84*, 379–393. [[CrossRef](#)]
7. Patel, R.L.; Sankhvara, C. Biodiesel production from Karanja oil and its use in diesel engine: A review. *Renew. Sustain. Energy Rev.* **2017**, *71*, 464–474. [[CrossRef](#)]

8. Tamjidi, S.; Esmaeili, H.; Moghadas, B.K. Performance of functionalized magnetic nanocatalysts and feedstocks on biodiesel production: A review study. *J. Clean. Prod.* **2021**, *305*, 127200. [[CrossRef](#)]
9. Vicente, G.; Martinez, M.; Aracil, J. Optimisation of integrated biodiesel production. Part I. A study of the biodiesel purity and yield. *Bioresour. Technol.* **2007**, *98*, 1724–1733. [[CrossRef](#)]
10. HadiNezhad, M.; Rowland, O.; Hosseini, F. The fatty acid profile and phenolic composition of *Descurainia sophia* seeds extracted by supercritical CO₂. *J. Am. Oil Chem. Soc.* **2015**, *92*, 1379–1390. [[CrossRef](#)]
11. Quah, R.V.; Tan, Y.H.; Mubarak, N.; Khalid, M.; Abdullah, E.; Nolasco-Hipolito, C. An overview of biodiesel production using recyclable biomass and non-biomass derived magnetic catalysts. *J. Environ. Chem. Eng.* **2019**, *7*, 103219. [[CrossRef](#)]
12. Wang, A.; Sudarsanam, P.; Xu, Y.; Zhang, H.; Li, H.; Yang, S. Functionalized magnetic nanosized materials for efficient biodiesel synthesis via acid–base/enzyme catalysis. *Green Chem.* **2020**, *22*, 2977–3012. [[CrossRef](#)]
13. Akhtar, M.T.; Ahmad, M.; Asma, M.; Munir, M.; Zafar, M.; Sultana, S.; Mujtaba, M.; Mohamed, A.; Kalam, M.A. Efficient Production of Wild and Non-Edible *Brassica juncea* (L.) Czern. Seed Oil into High-Quality Biodiesel via Novel, Green and Recyclable NiSO₄ Nano-Catalyst. *Sustainability* **2022**, *14*, 10188. [[CrossRef](#)]
14. Hosseini, S.A. Nanocatalysts for biodiesel production. *Arab. J. Chem.* **2022**, *15*, 104152. [[CrossRef](#)]
15. Bano, S.; Ganie, A.S.; Sultana, S.; Sabir, S.; Khan, M.Z. Fabrication and optimization of nanocatalyst for biodiesel production: An overview. *Front. Energy Res.* **2020**, *8*, 579014. [[CrossRef](#)]
16. Ali, M.A.; Al-Hydary, I.A.; Al-Hattab, T.A. Nano-magnetic catalyst CaO-Fe₃O₄ for biodiesel production from date palm seed oil. *Bull. Chem. React. Eng. Catal.* **2017**, *12*, 460–468. [[CrossRef](#)]
17. Baskar, G.; Selvakumari, I.A.E.; Aiswarya, R. Biodiesel production from castor oil using heterogeneous Ni doped ZnO nanocatalyst. *Bioresour. Technol.* **2018**, *250*, 793–798. [[CrossRef](#)]
18. Zheng, Y.; Yu, X.; Yang, J. Synthesis of CaO-CeO₂ catalysts by soft template method for biodiesel production. In Proceedings of the IOP Conference Series: Earth and Environmental Science, Jakarta, Indonesia, 23–24 October 2017; p. 012048.
19. Ebadinezhad, B.; Haghighi, M.; Zeinalzadeh, H. Carbon-templated meso-design of nanostructured CeAPSO-34 for biodiesel production from free fatty acid and waste oil. *Renew. Energy* **2022**, *195*, 716–733. [[CrossRef](#)]
20. Zandi-Atashbar, N.; Ensafi, A.A.; Ahoor, A.H. Nano-CeO₂/SiO₂ as an efficient catalytic conversion of waste engine oil into liquid fuel. *J. Clean. Prod.* **2017**, *166*, 1010–1019. [[CrossRef](#)]
21. Taghavizadeh Yazdi, M.E.; Nazarnezhad, S.; Mousavi, S.H.; Sadegh Amiri, M.; Darroudi, M.; Bains, F.; Kargozar, S. Gum tragacanth (GT): A versatile biocompatible material beyond borders. *Molecules* **2021**, *26*, 1510. [[CrossRef](#)]
22. Nejatian, M.; Abbasi, S.; Azarikia, F. Gum Tragacanth: Structure, characteristics and applications in foods. *Int. J. Biol. Macromol.* **2020**, *160*, 846–860. [[CrossRef](#)] [[PubMed](#)]
23. Akhtar, M.T.; Ahmad, M.; Shaheen, A.; Zafar, M.; Ullah, R.; Asma, M.; Sultana, S.; Munir, M.; Rashid, N.; Malik, K. Comparative study of liquid biodiesel from *Sterculia foetida* (bottle tree) using CuO-CeO₂ and Fe₂O₃ nano catalysts. *Front. Energy Res.* **2019**, *7*, 4. [[CrossRef](#)]
24. Ferrero, G.O.; Faba, E.M.S.; Rickert, A.A.; Eimer, G.A. Alternatives to rethink tomorrow: Biodiesel production from residual and non-edible oils using biocatalyst technology. *Renew. Energy* **2020**, *150*, 128–135. [[CrossRef](#)]
25. Velusamy, P.; Das, J.; Pachaiappan, R.; Vaseeharan, B.; Pandian, K. Greener approach for synthesis of antibacterial silver nanoparticles using aqueous solution of neem gum (*Azadirachta indica* L.). *Ind. Crops Prod.* **2015**, *66*, 103–109. [[CrossRef](#)]
26. Souza, M.C.G.; de Oliveira, M.F.; Vieira, A.T.; de Faria, A.M.; Batista, A.C.F. Methyl and ethyl biodiesel production from crambe oil (*Crambe abyssinica*): New aspects for yield and oxidative stability. *Renew. Energy* **2021**, *163*, 368–374. [[CrossRef](#)]
27. Borah, M.J.; Das, A.; Das, V.; Bhuyan, N.; Deka, D. Transesterification of waste cooking oil for biodiesel production catalyzed by Zn substituted waste egg shell derived CaO nanocatalyst. *Fuel* **2019**, *242*, 345–354. [[CrossRef](#)]
28. Navada, M.K.; Karnikkar, N.G.; D'Souza, J.N.; Kouser, S.; Aroor, G.; Kudva, J.; Jayappa, M.D. Biosynthesis of phyto functionalized cerium oxide nanoparticles mediated from *Scoparia dulcis* L. for appraisal of anti-cancer potential against adenocarcinomic lung cancer cells and paracetamol sensing potentiality. *Environ. Sci. Pollut. Res.* **2022**, 1–20. [[CrossRef](#)]
29. Ahmad, A.; Javed, M.S.; Khan, S.; Almutairi, T.M.; Mohammed, A.A.; Luque, R. Green synthesized Ag decorated CeO₂ nanoparticles: Efficient photocatalysts and potential antibacterial agents. *Chemosphere* **2023**, *310*, 136841. [[CrossRef](#)]
30. Irfan, M.; Munir, H.; Ismail, H. *Moringa oleifera* gum based silver and zinc oxide nanoparticles: Green synthesis, characterization and their antibacterial potential against MRSA. *Biomater. Res.* **2021**, *25*, 1–8. [[CrossRef](#)]
31. Anjum, F.; Gul, S.; Khan, M.I.; Khan, M.A. Efficient synthesis of palladium nanoparticles using guar gum as stabilizer and their applications as catalyst in reduction reactions and degradation of azo dyes. *Green Process. Synth.* **2020**, *9*, 63–76. [[CrossRef](#)]
32. Khaledi, K.; Haghighi, M.; Sadeghpour, P. On the catalytic properties and performance of core-shell ZSM-5@ MnO nanocatalyst used in conversion of methanol to light olefins. *Microporous Mesoporous Mater.* **2017**, *246*, 51–61. [[CrossRef](#)]
33. Akintelu, S.; Folorunso, A. Characterization and antimicrobial investigation of synthesized silver nanoparticles from *Annona muricata* leaf extracts. *J. Nanotechnol. Nanomed. Nanobiotechnol.* **2019**, *6*, 1–5.
34. Sethy, N.K.; Arif, Z.; Mishra, P.K.; Kumar, P. Green synthesis of TiO₂ nanoparticles from *Syzygium cumini* extract for photo-catalytic removal of lead (Pb) in explosive industrial wastewater. *Green Process. Synth.* **2020**, *9*, 171–181. [[CrossRef](#)]
35. Ala'a, H.; Osman, A.I.; Kumar, P.S.M.; Jamil, F.; Al-Haj, L.; Al Nabhani, A.; Kyaw, H.H.; Myint, M.T.Z.; Mehta, N.; Rooney, D.W. Circular economy approach of enhanced bifunctional catalytic system of CaO/CeO₂ for biodiesel production from waste loquat seed oil with life cycle assessment study. *Energy Convers. Manag.* **2021**, *236*, 114040.

36. Foroutan, R.; Peighambaroust, S.J.; Mohammadi, R.; Peighambaroust, S.H.; Ramavandi, B. Application of walnut shell ash/ZnO/K₂CO₃ as a new composite catalyst for biodiesel generation from *Moringa oleifera* oil. *Fuel* **2022**, *311*, 122624. [[CrossRef](#)]
37. Thangarasu, V.; Siddharth, R.; Ramanathan, A. Modeling of process intensification of biodiesel production from Aegle Marmelos Correa seed oil using microreactor assisted with ultrasonic mixing. *Ultrason. Sonochem.* **2020**, *60*, 104764. [[CrossRef](#)]
38. Abu-Ghazala, A.H.; Abdelhady, H.H.; Mazhar, A.A.; El-Deab, M.S. Valorization of hazard waste: Efficient utilization of white brick waste powder in the catalytic production of biodiesel from waste cooking oil via RSM optimization process. *Renew. Energy* **2022**, *200*, 1120–1133. [[CrossRef](#)]
39. Pang, D.; Tan, H.; Zhu, R.; Ouyang, F. Producing biodiesel from waste animal oil by modified ZnO. *Int. J. Green Energy* **2017**, *14*, 703–711. [[CrossRef](#)]
40. Attari, A.; Abbaszadeh-Mayvan, A.; Taghizadeh-Alisaraie, A. Process optimization of ultrasonic-assisted biodiesel production from waste cooking oil using waste chicken eggshell-derived CaO as a green heterogeneous catalyst. *Biomass Bioenergy* **2022**, *158*, 106357. [[CrossRef](#)]
41. Helmi, M.; Tahvildari, K.; Hemmati, A.; Azar, P.A.; Safekordi, A. Converting waste cooking oil into biodiesel using phosphomolybdic acid/clinoptilolite as an innovative green catalyst via electrolysis procedure; optimization by response surface methodology (RSM). *Fuel Process. Technol.* **2022**, *225*, 107062. [[CrossRef](#)]
42. Abd Malek, M.N.F.; Pushparaja, L.; Hussin, N.M.; Embong, N.H.; Bhuyar, P.; Rahim, M.H.A.; Maniam, G.P. Exploration of efficiency of nano calcium oxide (CaO) as catalyst for enhancement of biodiesel production. *J. Microbiol. Biotechnol. Food Sci.* **2021**, *11*, e3935. [[CrossRef](#)]
43. Munir, M.; Ahmad, M.; Saeed, M.; Waseem, A.; Nizami, A.-S.; Sultana, S.; Zafar, M.; Rehan, M.; Srinivasan, G.R.; Ali, A.M. Biodiesel production from novel non-edible caper (*Capparis spinosa* L.) seeds oil employing Cu–Ni doped ZrO₂ catalyst. *Renew. Sustain. Energy Rev.* **2021**, *138*, 110558. [[CrossRef](#)]
44. Rehan, M.; Gardy, J.; Demirbas, A.; Rashid, U.; Budzianowski, W.; Pant, D.; Nizami, A. Waste to biodiesel: A preliminary assessment for Saudi Arabia. *Bioresour. Technol.* **2018**, *250*, 17–25. [[CrossRef](#)] [[PubMed](#)]
45. Mendonça, I.M.; Paes, O.A.; Maia, P.J.; Souza, M.P.; Almeida, R.A.; Silva, C.C.; Duvoisin, S., Jr.; de Freitas, F.A. New heterogeneous catalyst for biodiesel production from waste tucumã peels (*Astrocaryum aculeatum* Meyer): Parameters optimization study. *Renew. Energy* **2019**, *130*, 103–110. [[CrossRef](#)]
46. Sandhya, R.; Velavan, R.; Ravichandran, J. Biodiesel production from waste cooking oil using copper doped zinc oxide nanocatalyst–process optimisation and economic analysis. *Int. J. Oil Gas Coal Technol.* **2020**, *25*, 488–497. [[CrossRef](#)]
47. Elkelay, M.; Bastawissi, H.A.-E.; Esmail, K.K.; Radwan, A.M.; Panchal, H.; Sadasivuni, K.K.; Ponnamma, D.; Walvekar, R. Experimental studies on the biodiesel production parameters optimization of sunflower and soybean oil mixture and DI engine combustion, performance, and emission analysis fueled with diesel/biodiesel blends. *Fuel* **2019**, *255*, 115791. [[CrossRef](#)]
48. Gupta, J.; Agarwal, M.; Dalai, A. Optimization of biodiesel production from mixture of edible and nonedible vegetable oils. *Biocatal. Agric. Biotechnol.* **2016**, *8*, 112–120. [[CrossRef](#)]
49. Munir, M.; Ahmad, M.; Mubashir, M.; Asif, S.; Waseem, A.; Mukhtar, A.; Saqib, S.; Munawaroh, H.S.H.; Lam, M.K.; Khoo, K.S. A practical approach for synthesis of biodiesel via non-edible seeds oils using trimetallic based montmorillonite nano-catalyst. *Bioresour. Technol.* **2021**, *328*, 124859. [[CrossRef](#)]
50. Chaudhry, B.; Akhtar, M.S.; Ahmad, M.; Munir, M.; Zafar, M.; Alhajeri, N.S.; Ala'a, H.; Ahmad, Z.; Hasan, M.; Bokhari, A. Membrane based reactors for sustainable treatment of *Coronopus didymus* L. by developing Iodine doped potassium oxide membrane under Dynamic conditions. *Chemosphere* **2022**, *303*, 135138. [[CrossRef](#)]
51. Chakraborty, M.; Baruah, D. Production and characterization of biodiesel obtained from *Sapindus mukorossi* kernel oil. *Energy* **2013**, *60*, 159–167. [[CrossRef](#)]
52. Atabani, A.; Shobana, S.; Mohammed, M.; Uğuz, G.; Kumar, G.; Arvindnarayan, S.; Aslam, M.; Ala'a, H. Integrated valorization of waste cooking oil and spent coffee grounds for biodiesel production: Blending with higher alcohols, FT–IR, TGA, DSC and NMR characterizations. *Fuel* **2019**, *244*, 419–430. [[CrossRef](#)]
53. Abdullah, R.F.; Rashid, U.; Hazmi, B.; Ibrahim, M.L.; Tsubota, T.; Alharthi, F.A. Potential heterogeneous nano-catalyst via integrating hydrothermal carbonization for biodiesel production using waste cooking oil. *Chemosphere* **2022**, *286*, 131913. [[CrossRef](#)]
54. Yahya, S.I.; Aghel, B. Estimation of kinematic viscosity of biodiesel-diesel blends: Comparison among accuracy of intelligent and empirical paradigms. *Renew. Energy* **2021**, *177*, 318–326. [[CrossRef](#)]
55. Seffati, K.; Honarvar, B.; Esmaili, H.; Esfandiari, N. Enhanced biodiesel production from chicken fat using CaO/CuFe₂O₄ nanocatalyst and its combination with diesel to improve fuel properties. *Fuel* **2019**, *235*, 1238–1244. [[CrossRef](#)]
56. Munir, M.; Saeed, M.; Ahmad, M.; Waseem, A.; Alsaady, M.; Asif, S.; Ahmed, A.; Khan, M.S.; Bokhari, A.; Mubashir, M. Cleaner production of biodiesel from novel non-edible seed oil (*Carthamus lanatus* L.) via highly reactive and recyclable green nano CoWO₃@rGO composite in context of green energy adaptation. *Fuel* **2023**, *332*, 126265. [[CrossRef](#)]
57. Zhukova, Y.; Studenyak, Y.; Mariychuk, R. New Indicators for Determination of Acid Number in Diesel Fuel Containing Biodiesel. In *Renewable Energy Sources: Engineering, Technology, Innovation*; Springer: Berlin/Heidelberg, Germany, 2020; pp. 431–443.
58. Khan, I.U.; Haleem, A.; Khan, A.U. Non-edible plant seeds of *Acacia farnesiana* as a new and effective source for biofuel production. *RSC Adv.* **2022**, *12*, 21223–21234. [[CrossRef](#)]

59. Pali, H.S.; Sharma, A.; Kumar, N.; Singh, Y. Biodiesel yield and properties optimization from Kusum oil by RSM. *Fuel* **2021**, *291*, 120218. [[CrossRef](#)]
60. Ahmad, M.; Zafar, M. Conversion of waste seed oil of *Citrus aurantium* into methyl ester via green and recyclable nanoparticles of zirconium oxide in the context of circular bioeconomy approach. *Waste Manag.* **2021**, *136*, 310–320.
61. Vasić, K.; Hojnik Podrepšek, G.; Knez, Ž.; Leitgeb, M. Biodiesel production using solid acid catalysts based on metal oxides. *Catalysts* **2020**, *10*, 237. [[CrossRef](#)]
62. Hoang, A.T. Prediction of the density and viscosity of biodiesel and the influence of biodiesel properties on a diesel engine fuel supply system. *J. Mar. Eng. Technol.* **2021**, *20*, 299–311. [[CrossRef](#)]
63. Abomohra, A.E.-F.; Almutairi, A.W. A close-loop integrated approach for microalgae cultivation and efficient utilization of agar-free seaweed residues for enhanced biofuel recovery. *Bioresour. Technol.* **2020**, *317*, 124027. [[CrossRef](#)]
64. Akubude, V.; Nwaigwe, K.; Dintwa, E. Production of biodiesel from microalgae via nanocatalyzed transesterification process: A review. *Mater. Sci. Energy Technol.* **2019**, *2*, 216–225. [[CrossRef](#)]
65. Schöggel, J.-P.; Stumpf, L.; Baumgartner, R.J. The narrative of sustainability and circular economy—A longitudinal review of two decades of research. *Resour. Conserv. Recycl.* **2020**, *163*, 105073. [[CrossRef](#)]
66. Mu, D.; Seager, T.P.; Rao, P.S.C.; Park, J.; Zhao, F. A resilience perspective on biofuel production. *Integr. Environ. Assess. Manag.* **2011**, *7*, 348–359. [[CrossRef](#)] [[PubMed](#)]
67. Sweetapple, C.; Fu, G.; Farmani, R.; Butler, D. Exploring wastewater system performance under future threats: Does enhancing resilience increase sustainability? *Water Res.* **2019**, *149*, 448–459. [[CrossRef](#)]
68. Giannetti, B.F.; Lopez, F.J.D.; Liu, G.; Agostinho, F.; Sevegnani, F.; Almeida, C.M. A Resilient and Sustainable World: Contributions from Cleaner Production, Circular Economy, Eco-innovation, Responsible Consumption, and Cleaner Waste Systems. *J. Clean. Prod.* **2022**, *384*, 135465. [[CrossRef](#)]
69. Gatto, A.; Drago, C. A taxonomy of energy resilience. *Energy Policy* **2020**, *136*, 111007. [[CrossRef](#)]

Disclaimer/Publisher's Note: The statements, opinions and data contained in all publications are solely those of the individual author(s) and contributor(s) and not of MDPI and/or the editor(s). MDPI and/or the editor(s) disclaim responsibility for any injury to people or property resulting from any ideas, methods, instructions or products referred to in the content.